Measurements-Based Channel Models for Indoor LiFi Systems

Measurements-Based Channel Models for Indoor LiFi Systems

Mohamed Amine Arfaoui*, Mohammad Dehghani Soltani, Iman Tavakkolnia, Ali Ghrayeb, Chadi Assi, Majid Safari, and Harald Haas

***Abstract*—Light-fidelity (LiFi) is a fully-networked bidirectional optical wireless communication (OWC) technology that is considered as a promising solution for high-speed indoor connectivity. Unlike in conventional radio frequency wireless systems, the OWC channel is not isotropic, meaning that the device orientation affects the channel gain significantly. However, due to the lack of proper channel models for LiFi systems, many studies have assumed that the receiver is vertically upward and randomly located within the coverage area, which is not a realistic assumption from a practical point of view. In this paper, novel realistic and measurement-based channel models for indoor LiFi systems are proposed. Precisely, the statistics of the channel gain are derived for the case of randomly oriented stationary and mobile users. For stationary users, two channel models are proposed, namely, the modified truncated Laplace (MTL) model and the modified Beta (MB) model. For mobile users, two channel models are proposed, namely, the sum of modified truncated Gaussian (SMTG) model and the sum of modified Beta (SMB) model. Based on the derived models, the impact of random orientation and spatial distribution of users is investigated, where we show that the aforementioned factors can strongly affect the channel gain and the system performance.**

***Index Terms*—Channel statistics, indoor channel models, light-fidelity (LiFi), Optical wireless communications, random waypoint, receiver orientation, receiver mobility.**

I. Introduction

A. Motivation

The total data traffic is expected to become about 49 exabytes per month by 2021, while in 2016, it was approximately 7.24 exabytes per month [1]. With this drastic increase, the fifth generation (5G) networks and beyond must urgently provide high data rates, seamless connectivity, robust security and ultra-low latency communications [2]–[4]. In addition, with the emergence of the internet-of-things (IoT) networks, the number of connected devices to the internet is increasing dramatically [5], [6]. This fact implies not only a significant increase in data traffic, but also the emergence of some IoT services with crucial requirements. Such requirements include high data rates, high connection density, ultra reliable low latency communication (URLLC) and security. However, traditional radio-frequency (RF) networks, which are already crowded, are unable to satisfy these high demands [7]. Network densification [8], [9] has been proposed as a solution to increase the capacity and coverage of 5G networks. However, with the continuous dramatic growth in data traffic, researchers from both industry and academia are trying to explore new network architectures, new transmission techniques and new spectra to meet these demands.

Light-fidelity (LiFi) is a novel bidirectional, high speed and fully networked optical wireless communication (OWC) technology, that uses visible light as the propagation medium in the downlink for the purposes of illumination and communication. It can use infrared in the uplink so that the illumination constraint of a room remains unaffected, and also to avoid interference with the visible light in the downlink [10]. LiFi offers a number of important benefits that have made it favorable for future networks. These include the very large, unregulated bandwidth available in the visible light spectrum (more than 2600 times greater than the whole RF spectrum), high energy efficiency [11], the straightforward deployment that uses off-the-shelf light emitting diode (LED) and photodiode (PD) devices at the transmitter and receiver ends, respectively, and enhanced security as light does not penetrate through opaque objects [12].

Going deep into LiFi technology, the authors in [13] studied the methods employed for enhancing the performance of LiFi systems, including modulation schemes and dimming control techniques. In [14], the authors focused on the LiFi link level transmission, the medium access techniques and the visible light sensing. Recently, the authors in [15] surveyed all the optimization techniques, previously reported in the literature, that aim to improve the performance of LiFi systems. Physical layer security for LiFi systems was also investigated in the literature [16], [17], where various information theoretic and signal processing techniques were proposed in order to enhance the secrecy performance of LiFi systems. Although LiFi technology was extensively studied, one of the key shortcomings of the current research literature on LiFi is the lack of appropriate statistical channel models for system design and handover management purposes.

B. Literature Review

In the context of this paper, we denote a LiFi user by one that is capable of communicating with an indoor LiFi system, i.e., the user equipment (UE) is equipped with a PD and hence can receive data signals from the LiFi access point (AP). Since the channel statistics of indoor LiFi systems depend mainly on the motion of users, we make a distinction between two main categories of users, namely, stationary and mobile

M. A. Arfaoui and C. Assi are with Concordia Institute for Information Systems Engineering (CIISE), Concordia University, Montreal, Canada, e-mail:{m_arfaou@encs, assi@ciise}.concordia.ca.

M. D. Soltani, I. Tavakkolnia, M. Safari and H. Haas are with the LiFi Research and Development Centre, Institute for Digital Communications, School of Engineering, University of Edinburgh, UK. e-mail: {m.dehghani, i.tavakkolnia, majid.safari, h.haas}@ed.ac.uk.

A. Ghrayeb is with the Electrical and Computer Engineering (ECE) department, Texas A&M University at Qatar, Doha, Qatar, e-mail: ali.ghrayeb@qatar.tamu.edu.

Corresponding author: M.A. Arfaoui, m_arfaou@encs.concordia.ca

users, depending on the their motion. A stationary user is a non-walking user, i.e., it has a fixed location through several consecutive time slots. On the other hand, a mobile user is a walking user, i.e., it moves over time, and hence, its location varies over several consecutive time slots.

Some statistical channel models for stationary and uniformly distributed users were proposed in [18]–[21], where a fixed incidence angle was assumed in [18]–[20] and a random incidence angle was assumed in [21]. However, accounting for mobility, which is an inherent feature of wireless networks, requires a more realistic and non-uniform model for users' spatial distribution. Several mobility models, such as the random waypoint (RWP) model, have been proposed in the literature to characterize the spatial distribution of mobile users for indoor RF systems [22], [23]. However, these studies were limited to RF spectrum where statistical fading channel models were used. Recently, [24], [25] employed the RWP mobility model to characterize the signal-to-noise ratio (SNR) for indoor LiFi systems. In [24], the device orientation was assumed constant over time, which is not a realistic scenario, whereas in [25], the incidence angle of optical signals was assumed to be uniformly distributed, which is not a proper model for the incidence angle, since it does not account for the actual statistics of device orientation.

The majority of studies on optical wireless communication (OWC) assume that the device always faces vertically upward. This assumption may have been driven by the lack of having a proper model for orientation, and/or to make the analysis tractable. Such an assumption is only accurate for a limited number of devices (e.g., laptops with a LiFi dongle), while the majority of users use devices such as smartphones, and in real-life scenarios, users tend to hold their device in a way that feels most comfortable. Such orientation can affect the users' throughput remarkably and it should be analyzed carefully. Even though a number of studies have considered the impact of random orientation in their analysis [26]–[33], all these studies assume a predefined model for the random orientation of the receiver. However, little or no evidence is presented to justify the assumed models. Nevertheless, none of these studies have considered the actual statistics of device orientation and have mainly assumed uniform or Gaussian distribution with hypothetical moments for device orientation. Recently, and for the first time, experimental measurements were carried out to model the polar and azimuth angles of the user's device in [34]–[37]. It is shown that the polar angle can be modeled by either a truncated Laplace distribution for the case of stationary users or a truncated Gaussian distribution for the case of mobile LiFi users, while the azimuth angle follows a uniform distribution for both cases. Motivated by these results, the impact of the random receiver orientation on the SNR and the bit error rate (BER) was studied for indoor stationary users in [38].

Solutions to alleviate the impact of device random orientation on the received SNR and throughput were proposed in [39]–[41]. In [39], the impact of the random receiver orientation, user mobility and blockage on the SNR and the BER was studied for indoor mobile users. Then, simulations of BER performance for spatial modulation using a multi-directional receiver configuration with consideration of random device orientation was evaluated. In [40], other multiple-input multiple-output (MIMO) techniques in the presence of random orientation were studied. The authors in [41], proposed an omni-directional receiver which is not affected by the device random orientation. It is shown that the omni-directional receiver reduces the SNR fluctuations and improves the user throughput remarkably. All these studies emphasize the significance of incorporating the random spatial distribution of users along with the random orientation of LiFi devices into the analysis. However, proper statistical channel models for indoor LiFi systems that encompass both the random spatial distribution and the random device orientation of users were not derived in the literature, which is the focus of this work.

C. Contributions and Outcomes

Against the above background, we investigate in this paper the channel statistics of indoor LiFi systems. Novel realistic and measurement-based channel models for indoor LiFi systems are proposed, and the proposed models encompass the random motion and device orientation of users. Precisely, the statistics of the line-of-sight (LOS) channel gain are derived for stationary and mobile users with random device orientation, using the measurements-based models of device orientation derived in [34]. For stationary users, the model of randomly located user is employed to characterize the spatial distribution of users, and the truncated Laplace distribution is used to model the device orientation. For mobile users, the RWP mobility model is used to characterize the spatial distribution of users and the truncated Gaussian distribution is used to model the device orientation. In light of the above discussion, we may summarize the paper contributions as follows.

- For stationary users, two channel models are proposed, namely the modified truncated Laplace (MTL) model and the modified Beta (MB) model. For mobile users, also two channel models are proposed, namely the sum of modified truncated Gaussian (SMTG) model and the sum of modified Beta (SMB) model. The accuracy of the derived models is then validated using the Kolmogorov-Smirnov distance (KSD) criterion.
- The BER performance of LiFi systems is investigated for both cases of stationary and mobile users using the derived statistical channel models. We show that the random orientation and the random spatial distribution of users could have strong effect on the error performance of LiFi systems.
- We propose a novel design of indoor LiFi systems that can alleviate the effects of random device orientation and random spatial distribution of users. We show that the proposed design is able to guarantee good error performance for LiFi systems under the realistic behaviour of users.
- The proposed statistical LiFi channel models are of great significance. In fact, any LiFi transceiver design, to be efficient, it needs to incorporate the channel model into the design. Therefore, having realistic channel models will help in designing realistic LiFi transceivers.

TABLE I
TABLE OF NOTATIONS

System Geometry	
R	Radius of the LiFi attocell
R_{e}	Radius of the large area
h_{a}	Height of the AP
h_{u}	Height of the LiFi receiver
LiFi Channel Parameters	
H	LOS channel gain
r	Polar distance of the user
α	Polar angle of the user
l	Distance from the AP to the user
Ω	Angle of the direction facing the user
θ	Elevation angle of the LiFi receiver
Ψ	Angle of incidence
Ψ_c	Field of view

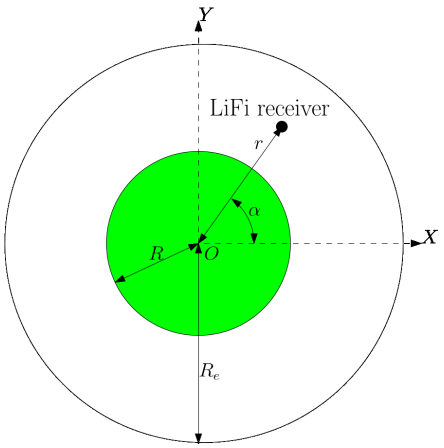

Fig. 1. Top view of a LiFi attocell which is concentric with a larger circular area.

D. Outline and Notations

The rest of the paper is organized as follows. The system model is presented in Section II. Section III presents the exact statistics of the LOS channel gain. In Sections IV, statistical channel models for stationary and mobile users are proposed. Finally, the paper is concluded in Section V and future research directions are highlighted.

The notations adopted throughout the paper are summarized in Table I. In addition, for every random variable X, f_X and F_X denote the probability density function (PDF) and the cumulative distribution function (CDF) of X, respectively. The function $\delta(\cdot)$ denotes the Dirac delta function. The function $\mathcal{U}_{[a,b]}(\cdot)$ denotes the the unit step function within $[a,b]$, i.e., for all $x \in \mathbb{R}$, $\mathcal{U}_{[a,b]}(x) = 1$ if $x \in [a,b]$, and 0 otherwise.

II. System Model

Consider the indoor LiFi cellular system shown in Fig. 1, which consists of a LiFi attocell with radius R (green attocell), that is equipped with a single AP installed at height h_{a} from the ground. The LiFi attocell is concentric with a larger circular area with a radius R_{e} ($R \leq R_{\mathrm{e}}$), within which a user may be located. The UE is equipped with a single PD that is used for communication with the AP. Assuming that the global coordinate system (O, X, Y, Z) is cylindrical, the coordinates of the UE are given by $(r, \alpha, h_{\mathrm{u}})$, where $r \in [0, R_{\mathrm{e}}]$ is the polar distance, $\alpha \in [0, 2\pi]$ is the polar angle and $h_{\mathrm{u}} \in [0, h_{\mathrm{a}}]$ is the height of the LiFi receiver. The user is assumed to hold the UE within a close distance of the body. Therefore, the polar coordinates (r, α) of the UE are assumed exactly the same as those of the user. However, this is not the case for the height h_{u}, since it depends mainly on the activity of the user, i.e., either stationary (sitting activity) or mobile (walking activity). Furthermore, in this communication model, the UE can be connected to the AP if it is located inside the LiFi attocell, i.e., when $r \leq R$. In this case, the received signal at the receiver at each channel use is expressed as

$$Y = HS + N, \tag{1}$$

where H is the downlink channel gain, S is the transmitted signal and N is an additive white Gaussian noise (AWGN) that is $\mathcal{N}(0, \sigma^2)$ distributed. Since LiFi signals should be positive valued and satisfy a certain peak optical power constraint [42], we assume that $0 \leq S \leq S_{\max}$, where $S_{\max} \in \mathbb{R}_+$ denotes the maximum allowed signal amplitude.

The channel gain H is typically the sum of a LOS component and non-light-of-sight (NLOS) components resulting from reflections off walls. Concerning the NLOS components, it was observed in [43], [44] that, when the LiFi AP is far from the walls, those components are insignificant as compared to the LOS component except when the receiver is very close to a corner in the indoor environment. In the system setup considered in this paper, which is shown in Fig. 1, we assume that the LiFi AP is relatively far from the walls of the indoor environment and we are interested in investigating the channel statistics of the LiFi attocell when the user is within its coverage area (the green area with radius R). In this case, the contribution of the NLOS components is negligible compared to that of the LOS component, and hence, only the LOS component is considered in our analysis.[1] Based on this, the channel gain H is expressed as [44]

$$H = H_0 \frac{\cos(\phi)^m \cos(\psi)}{l^2} \times \mathcal{U}_{[0,\Psi_c]}(\psi), \tag{2}$$

where, as shown in Fig. 2, m is the order of the Lambertian emission that is given by $m = \frac{-\log(2)}{\log(\cos(\phi_{1/2}))}$, such that $\phi_{1/2}$ represents the semi-angle of a LED; $l = \sqrt{r^2 + (h_{\mathrm{a}} - h_{\mathrm{u}})^2}$ is the distance between the AP and the UE; $\phi \in [0, \phi_{1/2}]$ is the radiation angle; $\psi \in [0, \pi]$ is the incidence angle and Ψ_c is the field of view of the PD. In (2), H_0 is expressed as

$$H_0 = \rho R_p \frac{(m+1)}{2\pi} \frac{n_c^2 A_g}{\sin(\Psi_c)^2}, \tag{3}$$

where ρ is the electrical-to-optical conversion factor of the LED, R_p is the PD responsivity, A_g is the geometric area of the PD and n_c is the refractive index of the PD's optical concentrator.

Based on the results of [34], $\cos(\phi)$ and $\cos(\psi)$ are

[1]The channel statistics of the total channel gain including both the LOS and the NLOS components will be considered in future work.

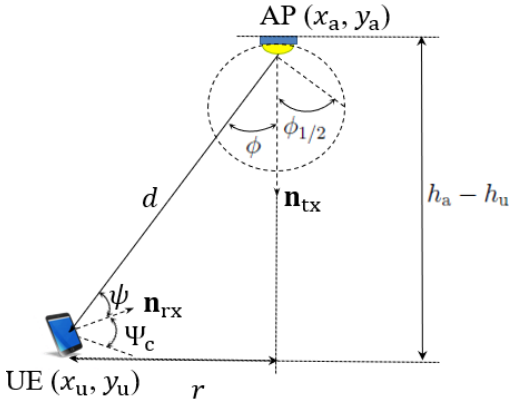

Fig. 2. Description of the indoor LiFi communication link.

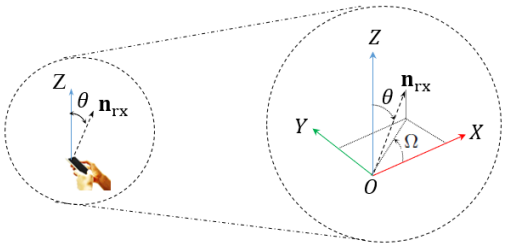

Fig. 3. Orientation angles of the LiFi receiver.

expressed, respectively, as

$$\cos(\phi) = \frac{h_a - h_u}{l}, \tag{4a}$$

$$\cos(\psi) = \frac{(z_a - z_u)}{l}\cos(\theta) - \frac{(x_a - x_u)}{l}\cos(\Omega)\sin(\theta) - \frac{(y_a - y_u)}{l}\sin(\Omega)\sin(\theta), \tag{4b}$$

where (x_a, y_a, z_a) and (x_u, y_u, z_u) are the Cartesian coordinates of the AP and the UE, respectively, and as shown in Fig. 3, Ω and θ are the angle of direction and the elevation angle of the UE, respectively. The angle of direction Ω represents the angle between the direction the user is facing and the X-axis, whereas the elevation angle θ is the angle between the normal vector of PD n_{rx} and the Z-axis. Based on Fig. 2, we have $(x_a, y_a, z_a) = (0, 0, h_a)$ and $(x_u, y_u, z_u) = (r\cos(\alpha), r\sin(\alpha), h_u)$. Therefore, $\cos(\psi)$ can be expressed as

$$\cos(\psi) = \frac{r\cos(\Omega - \alpha)\sin(\theta) + (h_a - h_u)\cos(\theta)}{l}. \tag{5}$$

Consequently, the LOS channel gain H is expressed as

$$H = \left(\frac{a(\theta)r}{l^{m+3}}\cos(\Omega - \alpha) + \frac{b(\theta)}{l^{m+3}}\right) \times \mathcal{U}_{[\cos(\Psi_c),0]}\left(\cos\left(\psi\right)\right), \tag{6}$$

where $a(\theta) = H_0(h_a - h_u)^m \sin(\theta)$ and $b(\theta) = H_0(h_a - h_u)^{m+1}\cos(\theta)$.

Based on the above, we conclude that the random behaviour of the channel gain H depends mainly on four random variables, which are r, α, Ω and θ. Precisely, the variables r and α model the randomness of the instantaneous location of the user whereas the variables Ω and θ model the randomness of the instantaneous UE orientation. Additionally, the statistics of the polar distance r and the the elevation angle θ depend on the motion of the user, either stationary or mobile. Consequently, the statistics of the LOS channel gain H inducibly depend on the user activity. In the following section, the exact statistics of the channel gain H are derived for the case of stationary and mobile users.

III. Channel Statistics of Stationary and Mobile users with Random Device orientation

The objective of this section is deriving the exact statistics of the LOS channel gain H for the case of stationary and mobile users. In subsection III-A, we present the statistics of the four main factors r, α, Ω and θ for each case, from which we derive in subsection III-B the exact statistics of H.

A. Parameters Statistics

From a statistical point of view, the instantaneous location and the instantaneous orientation of the UE are independent. Thus, the couples of random variables (r, α) and (Ω, θ) are independent. In addition, based on the results of [24], [45], the random variables r and α are independent, since r defines the polar distance and α defines the polar angle. On the other hand, based on the results of [34], the angle of direction Ω and the elevation angle θ are also statistically independent. Therefore, the random variables r, α, Ω and θ are independent. In addition, for both cases of stationary and mobile users, the random variables α and Ω are uniformly distributed within $[0, 2\pi]$ [24], [34], [45]. However, this is not the case for the polar distance r and the elevation angle θ. In fact, as we will show in the following, the statistics of r and θ depend on whether the user is stationary or mobile.

1) Stationary user:

When the user is stationary, its location is fixed. However, the user is randomly located, i.e., its instantaneous location is uniformly distributed within the circular area of radius R_e. It is important to mention that the user location is conditioned on the distribution of different objects existing within the indoor environment (e.g: desks, tables, closets). Such distribution of objects depends on various environmental factors and may vary from one indoor environment to the other. However, in the context of channel modeling, which was deeply investigated for the case of traditional RF and mmWave communications, one can remark that the goal is always to derive general channel statistics that can be applied independently from the propagation environment. Based on this, assuming a uniform spatial distribution for stationary users is a valid spatial distribution model, which was also adopted in a large body of works in the LiFi literature [20], [46], [47]. In this case, the PDF of the polar distance r is expressed as $f_r(r) = \frac{2r}{R_e^2}\mathcal{U}_{[0,R_e]}(r)$ [45]. On the other hand, the authors in [34] presented a measurement-based study for the UE orientation, where they derived statistical models for the elevation angle θ. In this study, they show that, for stationary users, the elevation angle

θ follows a truncated Laplace distribution, where its PDF is expressed as

$$f_\theta(\theta) = \frac{\exp\left(-\frac{|\theta-\mu_\theta|}{\sigma_\theta/\sqrt{2}}\right)\mathcal{U}_{[0,\pi/2]}(\theta)}{\sqrt{2\sigma_\theta}\left(1-\exp\left(-\frac{\left(\frac{\pi}{2}-\mu_\theta\right)}{\sigma_\theta/\sqrt{2}}\right)-\exp\left(-\frac{\mu_\theta}{\sigma_\theta/\sqrt{2}}\right)\right)}, \tag{7}$$

such that $\mu_\theta = 41.39^\circ$ and $\sigma_\theta = 7.68^\circ$.

2) Mobile user:

For a mobile user, and especially in indoor environments, the UE motion represents the user's walk, which is equivalent to a 2-D topology of the RWP mobility model, where the direction, velocity and destination points (waypoints) are all selected randomly. Based on [22], [23], the spatial distribution of the UE is polynomial in terms of the polar distance r and its PDF is expressed as $f_r(r) = \sum_{i=1}^{3} a_i \frac{r^{b_i}}{R_{\rm e}^{b_i+1}}\mathcal{U}_{[0,R_{\rm e}]}(r)$, where $[a_1, a_2, a_3] = \frac{1}{75}[324, -420, 96]$ and $[b_1, b_2, b_3] = [1, 3, 5]$. Moreover, it was shown in the same measurement-based study in [34] that, for a mobile user, the elevation angle θ follows a truncated Gaussian distribution, where its PDF is expressed as

$$f_\theta(\theta) = \frac{2\exp\left(-\frac{(\theta-\mu_\theta)^2}{2\sigma_\theta^2}\right)\mathcal{U}_{[0,\pi/2]}(\theta)}{\sqrt{2\pi\sigma_\theta^2}\left(\mathrm{erf}\left(\frac{\frac{\pi}{2}-\mu_\theta}{\sqrt{2}\sigma_\theta}\right)+\mathrm{erf}\left(\frac{\mu_\theta}{\sqrt{2}\sigma_\theta}\right)\right)}, \tag{8}$$

such that $\mu_\theta = 29.67^\circ$ and $\sigma_\theta = 7.78^\circ$.

B. Channel Statistics

As stated in Section II, the user can be located anywhere inside the outer circular area with radius $R_{\rm e}$. However, it is connected to the desired AP if it is located inside the LiFi attocell, i.e., if $r \in [0, R]$. In other words, in order to establish a communication link between the user and the desired AP, the only admitted values of the polar distance r should be within the range $[0, R]$. Due to this, we constrain the range of r to be $[0, R]$, and therefore, the exact PDF of the polar distance r becomes $\tilde{f}_r(r) = \frac{f_r(r)}{F_r(R)-F_r(0)}\mathcal{U}_{[0,R]}(r)$, where F_r denotes the CDF of r. Consequently, the PDF of the distance $l = \sqrt{r^2 + (h_a - h_u)^2}$ is given by

$$f_l(l) = \frac{l \times \tilde{f}_r\left(\sqrt{l^2-(h_a-h_u)^2}\right)}{\sqrt{l^2-(h_a-h_u)^2}}\mathcal{U}_{[l_{\min},l_{\max}]}(l), \tag{9}$$

where $l_{\min} = h_a - h_u$ and $l_{\max} = \sqrt{R^2 + (h_a - h_u)^2}$.

Now consider the random variable $\cos(\Omega - \alpha)$ appearing in (6). Since Ω and α are independent and uniformly distribution within $[0, 2\pi]$ and using the PDF transformation of random variables, $\cos(\Omega - \alpha)$ follows the arcsine distribution within the range $[-1, 1]$. Thus, the PDF and CDF of $\cos(\Omega - \alpha)$ are expressed, respectively, as

$$f_{\cos(\Omega-\alpha)}(x) = \frac{1}{\pi\sqrt{1-x^2}}\mathcal{U}_{[-1,1]}(x), \tag{10}$$

$$F_{\cos(\Omega-\alpha)}(x) = \left(\frac{\arcsin(x)}{\pi}+\frac{1}{2}\right)\mathcal{U}_{[-1,1]}(x) + \mathcal{U}_{[1,+\infty]}(x). \tag{11}$$

Based on this, the exact PDF of the channel gain H is given in the following theorem.

***Theorem* 1.** *The range of the LOS channel gain H is $[h_{\min}, h_{\max}]$, where $h_{\min} = 0$ and $h_{\max} = \frac{H_0}{(h_a-h_u)^2}$. In addition, for $h \in [h_{\min}, h_{\max}]$, the PDF of H is expressed as*

$$f_H(h) = g_H(h)\mathcal{U}_{\left[h^*_{\min},h_{\max}\right]}(h) + F_{\cos(\psi)}(\cos(\Psi_c))\delta(h), \tag{12}$$

where $h^*_{\min} = \frac{H_0(h_a-h_u)^m\cos(\Psi_c)}{l_{\max}^{m+2}}$, $F_{\cos(\psi)}(\cos(\Psi_c))$ is given in (13) on the top of the next page, in which $l^*_{\min}(h) = \max\left(l_0(h), l_{\min}\right)$ such that

$$l_0(h) = \left(\frac{h_0(h_a-h_u)^m\cos(\Psi_c)}{h}\right)^{\frac{1}{m+2}}, \tag{14}$$

and the function g_H is expressed as shown in (15) on the top of the next page, in which the function v is expressed as $v(h) = \frac{-(h_0(h_a-h_u)^m\cos(\Psi_c))^{\frac{1}{m+2}}}{(m+2)h^{\frac{m+3}{m+2}}}\mathcal{U}_{\left[h^*_{\min},h^*_{\max}\right]}$, such that $h^*_{\max} = \frac{H_0(h_a-h_u)^m\cos(\Psi_c)}{l_{\min}^{m+2}}$, and the function J_H is expressed as

$$J_H(\theta, l) = F_{\cos(\Omega-\alpha)}\left(\frac{l^*_{\min}\cos(\Psi_c)-(h_a-h_u)\cos(\theta)}{\sin(\theta)\sqrt{{l^*_{\min}}^2-(h_a-h_u)^2}}\right) - F_{\cos(\Omega-\alpha)}\left(\frac{{l^*_{\min}}^{m+3}h-b(\theta)}{a(\theta)\sqrt{{l^*_{\min}}^2-(h_a-h_u)^2}}\right). \tag{16}$$

Proof. See Appendix A. □

The exact CDF of the LOS channel gain H is also provided in (40) in Appendix A.

As it can be seen in Theorem 1, the closed-form expression of the exact PDF of the LOS channel gain H in (12) is neither straightforward nor tractable, since it involves some complex and atypical integrals. Due to this, in order to provide simple and tractable channel models for indoor LiFi systems, we propose in the following section some approximations for the PDF of H in (12), for both cases of stationary and mobile users.

IV. Approximate PDFs of the LOS Channel Gain

In this section, our objective is to derive some approximations for the PDF of H, starting from the results of Theorem 1. The cases of stationary and mobile users are investigated separately in subsections IV-A and IV-B, respectively.

A. Stationary user

An approximate expression of the PDF of the LOS channel gain H for the case of a stationary user is given in the following theorem.

***Theorem* 2.** *For the case of a stationary user, an approximate expression of the PDF of the channel gain H is given by*

$$f_H(h) \approx \frac{1}{h^\nu}g(h) + F_{\cos(\psi)}(\cos(\Psi_c))\delta(h), \tag{17}$$

where $\nu > 0$ and g is a function with range $[h^*_{\min}, h_{\max}]$.

Proof. See Appendix B. □

$$F_{\cos(\psi)}(\cos(\Psi_c)) = \int_{l_{\min}}^{l_{\max}} \int_0^{\frac{\pi}{2}} F_{\cos(\Omega-\alpha)}\left(\frac{d\cos(\Psi_c) - (h_a - h_u)\cos\theta}{\sin(\theta)\sqrt{l^2 - (h_a - h_u)^2}}\right) f_\theta(\theta)\mathrm{d}\theta f_l(l)\mathrm{d}l \tag{13}$$

$$\begin{aligned} g_H(h) = &\int_{l^*_{\min}(h)}^{l_{\max}} \int_0^{\frac{\pi}{2}} \frac{l^{m+3}}{a(\theta)\sqrt{l^2 - (h_a - h_u)^2}} f_{\cos(\Omega-\alpha)}\left(\frac{l^{m+3}h - b(\theta)}{a(\theta)\sqrt{l^2 - (h_a - h_u)^2}}\right) f_\theta(\theta) f_l(l)\mathrm{d}\theta\mathrm{d}l \\ &+ v(h)\int_0^{\frac{\pi}{2}} J_H(\theta, l)\, f_\theta(\theta) f_l(l)\mathrm{d}\theta\mathrm{d}l, \end{aligned} \tag{15}$$

$$G_1(\gamma, \mu_H, b_H) = -b_H^{1+\gamma} e^{\frac{-\mu_H}{b_H}}\left[\Gamma\left(1+\gamma, \frac{h_{\max}}{b_H}\right) - \Gamma\left(1+\gamma, \frac{\mu_H}{b_H}\right) + (-1)^{1-\gamma}\left(\Gamma\left(1+\gamma, -\frac{\mu_H}{b_H}\right) - \Gamma\left(1+\gamma, -\frac{h^*_{\min}}{b_H}\right)\right)\right], \tag{20}$$

The approximation of the PDF of the LOS channel gain H provided in Theorem 2 expresses two main factors, which are the random location of the user and the random orientation of the UE. The functions $h \mapsto \frac{1}{h^\nu}$ and $h \mapsto g(h)$ express respectively the effects of the random location of the user and the random orientation of the UE on the LOS channel gain H. At this point, the missing part is the function g that provides the best approximation for the PDF of the LOS channel gain f_H. In the following, we provide two approximate expressions for the PDF g.

1) The Modified Truncated Laplace (MTL) Model:

Since the function $h \mapsto g(h)$ expresses the effect of the random orientation of UE on the LOS channel gain H and motivated by the fact that the elevation angle θ follows a truncated Laplace distribution as shown in (7), one reasonable choice for g is the Laplace distribution. Consequently, an approximate expression of the PDF of the LOS channel gain H can be given by

$$\begin{aligned} f_H(h) \approx &\frac{h^{-\nu}\exp\left(-\frac{|h-\mu_H|}{b_H}\right)}{M_1(-\nu, \mu_H, b_H)}\mathcal{U}_{[h^*_{\min}, h_{\max}]}(h) \\ &+ F_{\cos(\psi)}(\cos(\Psi_c))\delta(h), \end{aligned} \tag{18}$$

where $\mu_H \in [h^*_{\min}, h_{\max}]$, $b_H > 0$ and $M_1(-\nu, \mu_H, b_H)$ is a normalization factor given by

$$M_1(-\nu, \mu_H, b_H) = \frac{G_1(-\nu, \mu_H, b_H)}{\left[1 - F_{\cos(\psi)}(\cos(\Psi_c))\right]}, \tag{19}$$

in which G_1 is given in (20) on top of next page, such that Γ denotes the upper incomplete Gamma function. At this stage, we need to determine the parameters (ν, μ_H, b_H) of f_H. One approach to do this is through moments matching. Using the exact PDF of H in (12), the non-centered moments of the LOS channel gain H are given by

$$m_i^e = \int_{h^*_{\min}}^{h_{\max}} h^i g_H(h)\mathrm{d}h + F_{\cos(\psi)}(\cos(\Psi_c)), \quad i \in \mathbb{N}, \tag{21}$$

whereas by using the approximate PDF of H in (18), the non-centered moments of the LOS channel gain H are given by

$$m_i^a(\nu, \mu_H, b_H) = \frac{M_1(i-\nu, \mu_H, b_H)}{M_1(-\nu, \mu_H, b_H)}, \quad i \in \mathbb{N}, \tag{22}$$

Therefore, since only three parameters need to be determined, which are (ν, μ_H, b_H), they can be obtained by solving the following system of equations

$$m_i^a(\nu, \mu_H, b_H) = m_i^e, \quad \text{for } i = 1, 2, 3. \tag{23}$$

2) The Modified Beta (MB) Model:

The exact PDF of the LOS channel gain H involves the integral of a function that has the form $(x, y) \mapsto f_{\cos(\Omega-\alpha)}(g(x, y))$. Since $\cos(\Omega - \alpha)$ follows the arcsine distribution and based on the fact that the arcsine distribution is a special case of the Beta distribution, we approximate the function g with a Beta distribution. Consequently, an approximate expression of the PDF of the LOS channel gain H can be given by

$$\begin{aligned} &f_H(h) \\ &\approx \frac{h^{-\nu}\left(\frac{h-h^*_{\min}}{h_{\max}-h^*_{\min}}\right)^{\alpha_H-1}\left(\frac{h_{\max}-h}{h_{\max}-h^*_{\min}}\right)^{\beta_H-1}}{M_2(-\nu, \alpha_H, \beta_H)}\mathcal{U}_{[h^*_{\min}, h_{\max}]}(h) \\ &+ F_{\cos(\psi)}(\cos(\Psi_c))\delta(h), \end{aligned} \tag{24}$$

where $\alpha_H > 0$, $\beta_H > 0$ and $M_2(-\nu, \alpha_H, \beta_H)$ is a normalization factor given by

$$M_2(-\nu, \alpha_H, \beta_H) = \frac{G_2(-\nu, \alpha_H, \beta_H)}{\left[1 - F_{\cos(\psi)}(\cos(\Psi_c))\right]}, \tag{25}$$

such that G_2 is given in (26) at the top of the next page, in which ${}_2\tilde{F}_1$ denotes the regularized hyper-geometric function and

$$B(\gamma, \alpha_H, \beta_H) = \frac{\pi h_{\max}^{\beta_H-1}(h_{\max} - h^*_{\min})^{-\alpha_H-\beta_H+2}}{\sin(\pi(\alpha_H+\gamma))\Gamma(-\gamma)\Gamma(\alpha_H+\beta_H+\gamma)}. \tag{27}$$

Based on the above, it remains to derive the parameters (ν, α_H, β_H) of f_H. Similar to the case of the MTL model, one approach to do this is through moments matching. Specifically, (ν, α_H, β_H) can be obtained by solving the system of equations in (23), where for $i = 1, 2, 3$, m_i^a is expressed in this case as

$$m_i^a(\nu, \mu_H, b_H) = \frac{M_2(i-\nu, \alpha_H, \beta_H)}{M_2(-\nu, \alpha_H, \beta_H)}, \quad i \in \mathbb{N}. \tag{28}$$

$$G_2(\gamma,\alpha_H,\beta_H)=B(\gamma,\alpha_H,\beta_H)\times\left[\Gamma(\beta_H)\Gamma(-\gamma)h_{\max}^{\alpha_H+\gamma}{}_2\tilde{F}_1\left(1-\alpha_H,-\alpha_H-\beta_H-\gamma+1;-\alpha_H-v+1;\frac{h_{\min}^*}{h_{\max}}\right)\right.$$
$$\left.-\Gamma(\alpha_H)h_{\min}^{*\alpha_H+\gamma}\Gamma(\alpha_H+\beta_H+\gamma)_2\tilde{F}_1\left(1-\beta_H,\gamma+1;\beta_H+\gamma+1;\frac{h_{\min}^*}{h_{\max}}\right)\right], \tag{26}$$

B. Mobile users

An approximate expression of the PDF of the LOS channel gain H for the case of a mobile user is given in the following theorem.

***Theorem* 3.** *For the case of a mobile user, an approximate expression of the PDF of the channel gain H is given by*

$$f_H(h)\approx\sum_{j=1}^{3}\frac{1}{h^{\nu_i}}g_j(h)+F_{\cos(\psi)}(\cos(\Psi_c))\delta(h), \tag{29}$$

where, for $j=1,2,3$, $\nu_j>0$ and g_j is a function with range $[h_{\min}^*,h_{\max}]$.

Proof. See Appendix C. □

It is important to highlight here that, for $j=1,2,3$, the functions $h\mapsto\frac{1}{h^{\nu_j}}$ and $h\mapsto g_j(h)$ express respectively the effects of the user mobility and the random orientation of the UE on the LOS channel gain H. At this point, the missing part is the functions g_j, for $j=1,2,3$, that provide the best approximation for the PDF of the LOS channel gain f_H. In the following, we provide two expressions for each function g_j for $j=1,2,3$.

1) The Sum of Modified Truncated Gaussian (SMTG) Model:

Since for $j=1,2,3$, the functions $h\mapsto g_j(h)$ express the effect of the random orientation of the UE on the channel gain H and motivated by the fact that, for the case of mobile users, the elevation angle θ follows a truncated Gaussian distribution as shown in (8), one reasonable choice for the functions g_j is the truncated Gaussian distribution. Consequently, an approximate expression of the PDF of the LOS channel gain H can be given by

$$f_H(h)\approx\frac{\sum_{j=1}^{3}h^{-\nu_j}\exp\left(-\frac{(h-\mu_{H,j})^2}{2\sigma_{H,j}^2}\right)}{\sum_{j=1}^{3}M_3\left(-\nu_j,\mu_{H,j},\sigma_{H,j}\right)}\mathcal{U}_{[h_{\min}^*,h_{\max}]}(h)+F_{\cos(\psi)}(\cos(\Psi_c))\delta(h), \tag{30}$$

where for $j=1,2,3$, $\mu_{H,j}\in[h_{\min}^*,h_{\max}]$, $\sigma_{H,j}>0$ and $M_3\left(-\nu_j,\mu_{H,j},\sigma_{H,j}\right)$ is a normalization factor that is given by

$$M_3\left(-\nu_j,\mu_{H,j},\sigma_{H,j}\right)=\frac{\int_{h_{\min}^*}^{h_{\max}}h^{-\nu_j}\exp\left(-\frac{(h-\mu_{H,j})^2}{2\sigma_{H,j}^2}\right)\mathrm{d}h}{\left[1-F_{\cos(\psi)}(\cos(\Psi_c))\right]}. \tag{31}$$

Now, in order to to have the complete closed-form expression of f_H, we have to determine the parameters $\{(\nu_j,\mu_{H,j},b_{H,j}),j=1,2,3\}$. Similar to the one of the stationary users case, one approach to determine these parameters is through moments matching. Specifically, since only nine parameters need to be determined, which are $\{(\nu_j,\mu_{H,j},\sigma_{H,j})\,|j=1,2,3\}$, they can be obtained by solving the following system of equations

$$m_i^a=m_i^e,\quad\text{for } i=1,2,..,9, \tag{32}$$

where, for $i=1,2,...,9$, m_i^a is expressed in this case as

$$m_i^a=\frac{\sum_{j=1}^{3}M_3\left(i-\nu_j,\mu_{H,j},b_{H,j}\right)}{\sum_{j=1}^{3}M_3\left(-\nu_j,\mu_{H,j},\sigma_{H,j}\right)}. \tag{33}$$

2) The Sum of Modified Beta (SMB) Model:

Motivated by the same reasons as for the MB model in Section IV-A1, we approximate each function g_j, for $j=1,2,3$, with a Beta distribution. Consequently, an approximate expression of the PDF of the LOS channel gain H is given in (34) at the top of the next page, where $\alpha_{H,j}>0$, $\beta_{H,j}>0$ and $M_2\left(-\nu_j,\alpha_{H,j},\beta_{H,j}\right)$ is given in (25). Finally, it remains now to derive the parameters $\{(\nu_j,\alpha_{H,j},\beta_{H,j})\,|j=1,2,3\}$ of f_H. Similar to the STMG model, these parameters can be obtained by solving the system of equations in (32), where for $i=1,2,...,9$, m_i^a is expressed in this case as

$$m_i^a=\frac{\sum_{j=1}^{3}M_2\left(i-\nu_j,\alpha_{H,j},\beta_{H,j}\right)}{\sum_{j=1}^{3}M_2\left(-\nu,\alpha_H,\beta_H\right)}. \tag{35}$$

As a summary, a detailed algorithm for implementing the proposed statistical channel models for indoor LiFi systems is presented in Algorithm 1.

TABLE II
SIMULATION PARAMETERS

Parameter	Symbol	Value
Ceiling height	h_a	2.4 m
LED half-power semiangle	$\phi_{1/2}$	60°
LED conversion factor	ρ	0.7 W/A
PD responsivity	R_p	0.6 A/W
PD geometric area	A_g	1 cm^2
Optical concentrator refractive index	n_c	1
UE's height (stationary)	h_u	0.9 m
UE's height (mobile)	h_u	1.4 m

V. SIMULATION RESULTS AND DISCUSSIONS

In this paper, we consider a typical indoor LiFi attocell [24], [25]. Parameters used throughout the paper are shown in Table II. In Subsection V-A, we present the PDF and CDF of the LOS channel gain H for the case of stationary and mobile users. In Subsection V-B, we investigate the error performance of Indoor LiFi systems using the derived statistics of the LOS channel gain H. Finally, based on the error performance presented in V-B, we propose in subsection V-C an optimized design for the indoor cellular system that can enhance the error performance of LiFi systems.

$$f_H(h) \approx \frac{\sum_{j=1}^{3} h^{-\nu_j} \left(\frac{h-h^*_{\min}}{h_{\max}-h^*_{\min}}\right)^{\alpha_{H,j}-1} \left(\frac{h_{\max}-h}{h_{\max}-h^*_{\min}}\right)^{\beta_{H,j}-1} \mathcal{U}_{[h^*_{\min},h_{\max}]}(h)}{\sum_{j=1}^{3} M_2\left(-\nu_j, \alpha_{H,j}, \beta_{H,j}\right)} + F_{\cos(\psi)}(\cos(\Psi_c))\delta(h), \tag{34}$$

Algorithm 1 Detailed algorithm for implementing the proposed statistical channel models

1. **Input**:
   i) Attocell dimensions $(R, h_{\rm a})$.
   ii) AP's parameters $(\rho, \phi_{1/2})$.
   iii) UE's height $h_{\rm u}$
   iv) UE's parameters $(R_{\rm p}, n_{\rm c}, A_{\rm g}, \Psi_c)$.
2. **Calculate** H_0 as shown in (3).
3. **Calculate** $F_{\cos(\psi)}(\cos(\Psi_c))$ as shown in (13).
4. **If** the user is stationary:
   i) MTL model:
      a) Estimate the parameters using (23).
      b) Inject the parameters into the PDF in (18).
   ii) MB model:
      a) Estimate the parameters using (23).
      b) Inject the parameters into the PDF in (24).
   elseif the user is mobile:
   i) SMTG model:
      a) Estimate the parameters using (32).
      b) Inject the parameters into the PDF in (30).
   ii) SMB model:
      a) Estimate the parameters using (32).
      b) Inject the parameters into the PDF in (35).
   end

A. Channel Statistics

For stationary users, Figs. 4 and 5 present the exact, simulated and approximated PDF and CDF of the LOS channel gain H, when a radius of the attocell $R = 1$m and $R = 2.5$m, respectively. For both cases, two different values for the field of view of the UE were considered, which are $\Psi_c = 90°$ and $60°$. These figures show that the proposed MTL and MB models offer good approximation for the distribution of the LOS channel gain H. Analytically, in order to evaluate the goodness of the proposed MTL and MB models, we use the well-known Kolmogorov-Smirnov distance (KSD) [48]. In fact, the KSD measures the absolute distance between two distinct CDFs F_1 and F_2 [48], i.e.,

$$\text{KSD} = \max_x |F_1(x) - F_2(x)|. \tag{36}$$

Obviously, smaller values of the KSD correspond to more similarity between distributions. In our case, the KSD of the MTL and MB models are shown in Table III. As it can be seen in this table, the maximum KSD value for the MTL and MB models are 0.0669 and 0.0444, respectively, which demonstrates the good approximation offered by the MTL and MB models.

For mobile users, Figs. 6 and 7 present the exact, simulated and approximated PDF and CDF of the LOS channel gain H,

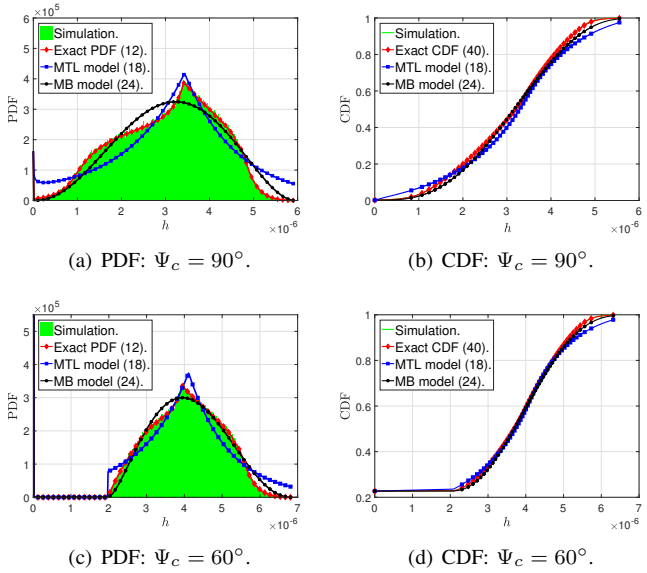

(a) PDF: $\Psi_c = 90°$. (b) CDF: $\Psi_c = 90°$.

(c) PDF: $\Psi_c = 60°$. (d) CDF: $\Psi_c = 60°$.

Fig. 4. The simulated, exact and approximated PDF and the CDF of the LOS channel gain H for the case of stationary users when $R = 1$ m.

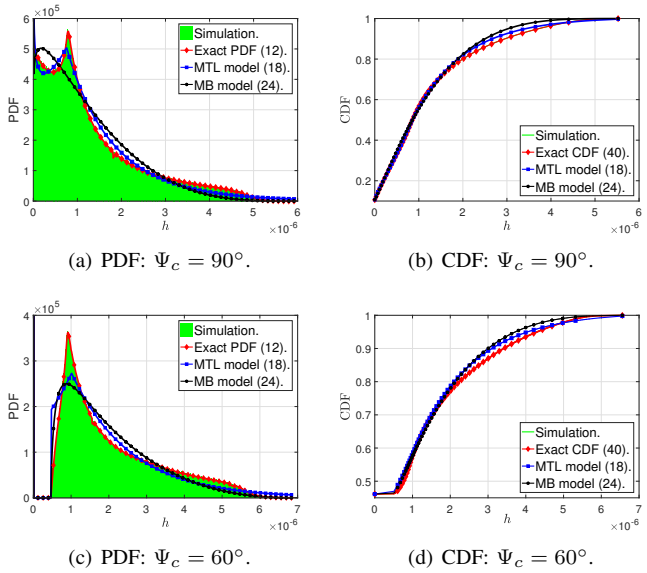

(a) PDF: $\Psi_c = 90°$. (b) CDF: $\Psi_c = 90°$.

(c) PDF: $\Psi_c = 60°$. (d) CDF: $\Psi_c = 60°$.

Fig. 5. The simulated, exact and approximated PDF and the CDF of the LOS channel gain H for the case of stationary users when $R = 2.5$ m.

when the radius of the attocell is $R = 1$m and $R = 2.5$m, respectively. For both cases, two different values for the field of view of the UE were considered, which are $\Psi_c = 90°$ and $60°$. These figures show that the proposed SMTG and SMB models offer good approximation for the distribution of the LOS channel gain H. Nevertheless, Table IV presents the KSD of the SMTG and the SMB models, where it shows that their maximum KSD values are 0.0238 and 0.0054, respectively.

TABLE III
KSD OF MTL AND MB MODELS

	MTL model		MB model	
	$\Psi_c = 90°$	$\Psi_c = 60°$	$\Psi_c = 90°$	$\Psi_c = 60°$
$R = 1$ m	0.0669	0.0448	0.0336	0.0197
$R = 2.5$ m	0.0239	0.0241	0.0444	0.0316

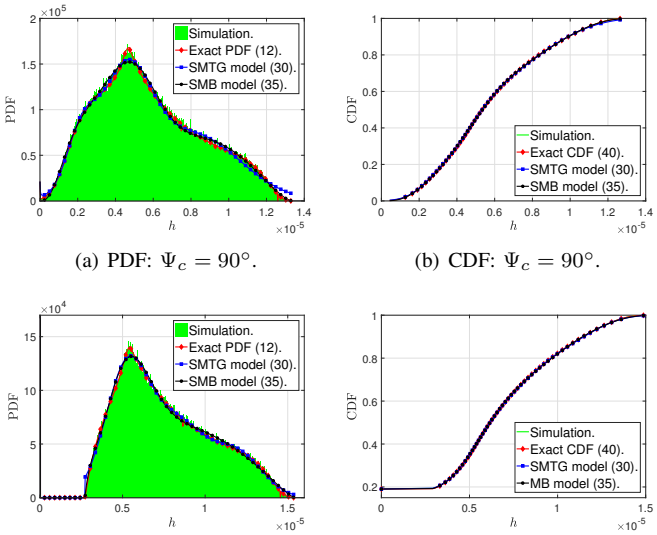

(a) PDF: $\Psi_c = 90°$. (b) CDF: $\Psi_c = 90°$.

(c) PDF: $\Psi_c = 60°$. (d) CDF: $\Psi_c = 60°$.

Fig. 6. The simulated, exact and approximated PDF and the CDF of the LOS channel gain H for the case of stationary users when $R = 1$ m.

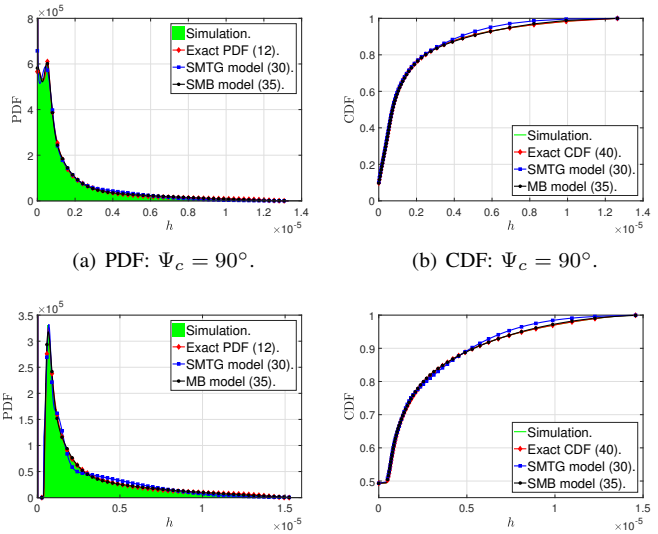

(a) PDF: $\Psi_c = 90°$. (b) CDF: $\Psi_c = 90°$.

(c) PDF: $\Psi_c = 60°$. (d) CDF: $\Psi_c = 60°$.

Fig. 7. The simulated, exact and approximated PDF and the CDF of the LOS channel gain H for the case of stationary users when $R = 2.5$ m.

TABLE IV
KSD OF SMTG AND SMB MODELS

	SMTG model		SMB model	
	$\Psi_c = 90°$	$\Psi_c = 60°$	$\Psi_c = 90°$	$\Psi_c = 60°$
$R = 1$ m	0.0082	0.0037	0.0048	0.0030
$R = 2.5$ m	0.0238	0.0156	0.0054	0.0047

These results demonstrate the good approximation offered by the SMTG and SMB models.

As it can be seen in Figs. 4-7, one can remark that the accuracy of the SMTG and SMB models, relative to the case of mobile users, provide better accuracy than the MTL and MB models, which are associated with the case of stationary users. This occurs mainly because for mobile users, the approximated PDF given in (29) is a mixture of three PDFs with nine parameters in total, whereas for the case of stationary users, the approximated PDF given in (17) is a single PDF expression with only three parameters in total. However, this better accuracy comes with a higher complexity, since for the MTL and MB models, we only need to estimate three parameters, whereas for the SMTG and SMB models, we need to estimate nine parameters.

B. Error Performance

Figs. 8(a) and 8(b) present the average BER performance of the on-off keying (OOK) modulation versus the transmitted optical power P_{opt} for stationary users, when the radius of the attocell $R = 1$m and 2.5m and when the field of view of the UE $\Psi_c = 90°$ and $60°$. These figures shows that the BER results of the MTL and MB models match perfectly the simulated BER for both cases when $(R, \Psi_c) = (2.5\text{m}, 90°)$ and when $\Psi_c = 60°$. However, for the case when $(R, \Psi_c) = (1\text{m}, 90°)$, we remark that the average BER results of the MB model match the simulated BER better than the ones of the MTL model. This can be also seen from the values of the KSD in Table III, where we can see that the KSD of the MB model is lower than the one of the MTL model when $(R, \Psi_c) = (1\text{m}, 90°)$. In other words, when $(R, \Psi_c) = (1\text{m}, 90°)$, the MB model offers better accuracy than the MTL model. This is mainly due to the assumptions made for both models. In fact, when the radius of the attocell R is small and by referring to (5), the random variable $\cos(\Omega - \alpha)$ is dominant in $\cos(\psi)$. Hence, assuming that the distribution of the random orientation of the UE can be approximated by a Beta distribution makes more sense.

Figs. 8(c) and 8(d) present the average BER performance of the OOK modulation versus the transmitted optical power P_{opt} for mobile users, when the radius of the attocell $R = 1$m and 2.5m and when the field of view of the UE $\Psi_c = 90°$ and $60°$. These figures show that the BER results of the SMTG and the SMB models match perfectly the simulated BER for both cases when $(R, \Psi_c) = (2.5\text{m}, 90°)$ and when $\Psi_c = 60°$. However, for the case when $(R, \Psi_c) = (1\text{m}, 90°)$, we remark that the BER results of the SMB model matches the simulated BER better than the ones of the SMTG model. Similar to the case of stationary users, the SMB model offers better accuracy than the SMTG model when $(R, \Psi_c) = (1\text{m}, 90°)$ due to the assumptions made for both models.

In order to give insights about the different factors that affects the error performance of LiFi systems, we consider for comparison purposes the following three baseline scenarios.

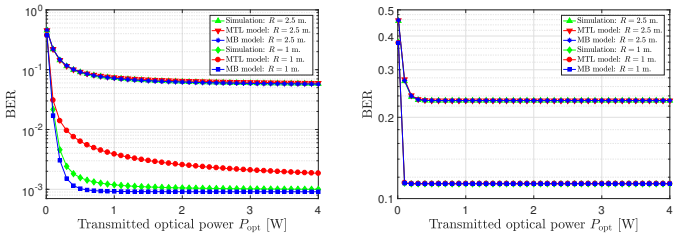

(a) Stationary user, $\Psi_c = 90$.

(b) Stationary user, $\Psi_c = 60°$.

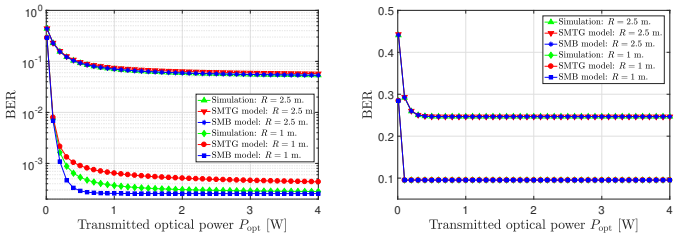

(c) Mobile user, $\Psi_c = 90°$.

(d) Mobile user, $\Psi_c = 60°$.

Fig. 8. BER performance of OOK modulation versus the transmitted optical power for stationary and mobile users.

- *Baseline 1:* fixed orientation with elevation angle $\theta = 0°$. This benchmark was considered in [20] for stationary users and in [24] for mobile users.
- *Baseline 2:* fixed radial location with polar distance $r = 0$ m.
- *Baseline 3:* fixed radial location with polar distance $r = R$.

Fig. 9 presents the bit-error-rate (BER) of the OOK modulation of our proposed channel models and of the aforementioned baselines versus the transmitted optical power for a UE with a field of view $\Psi_c = 90°$ in a LiFi attocell with a radius $R = 1$ m. This figure demonstrates the effects of the random motion if the user and the random orientation the UE in the error performance of LiFi systems. In fact, for the considered simulation setup and for both cases of stationary and mobile users, Fig. 9 shows that a target bit-error-rate of 10^{-4} can not be achieved due to these two factors. Hence, while designing indoor LiFi systems, these effects should be compensated with cooperative transmission techniques such as the coordinated broadcasting between LiFi APs.

Fig. 8 and Fig. 9 show also two important facts about the BER performance of users. First, it can be seen that the BER performance degrades heavily when either the radius of the attocell R increases or the field of view of the UE decreases. Second, the BER saturates as the transmitted optical power increases. These two facts can be explained by the following corollary.

***Corollary* 1.** *At high transmitted optical power P_{opt}, the average probability of error of the M-ary pulse amplitude modulation (PAM) for the considered LiFi system is given by*

$$\lim_{P_{\text{opt}} \to \infty} P_e\left(P_{\text{opt}}\right) = \frac{F_{\cos(\psi)}(\cos(\Psi_c))}{2}. \tag{37}$$

Proof. See appendix D. □

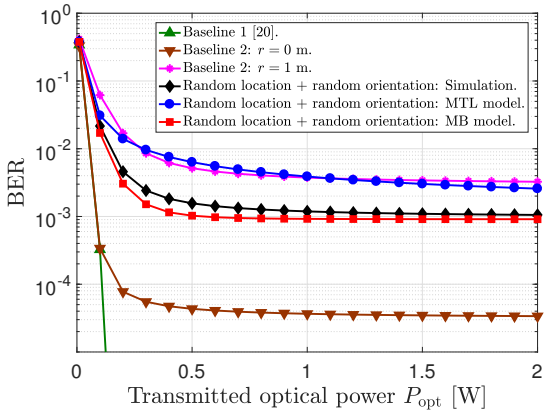

(a) Stationary user.

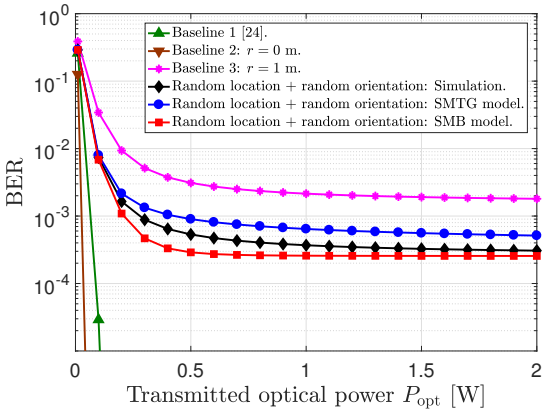

(b) Mobile user.

Fig. 9. BER performance of the OOK modulation, versus the transmitted optical power, of our proposed channel models and of the aforementioned baselines for a user with a field of view $\Psi_c = 90°$ in a LiFi attocell with a radius $R = 1$m.

The result of Corollary 1 shows that, even when the transmitted optical power P_{opt} is high, the BER is stagnating at $\frac{F_{\cos(\psi)}(\cos(\Psi_c))}{2}$. This result is directly related to the cases when the AP is out of the FOV of the UE. On the other hand, based on its expression in (13), $F_{\cos(\psi)}(\cos(\Psi_c))$ is a function of the attocell radius R and the field of view of the receiver Ψ_c. Therefore, since $l_{\max}$ increases as R increases, then $F_{\cos(\psi)}(\cos(\Psi_c))$ is an increasing function in R. In addition, since $x \mapsto F_{\cos(\psi)}(x)$ is a CDF, it is an increasing function, and due to the fact that $x \mapsto \cos(x)$ is a decreasing function within $[0, \pi/2]$, then $F_{\cos(\psi)}(\cos(\Psi_c))$ increases as Ψ_c decreases. The aforementioned reasons explain the poor BER performance of the LiFi system when either the radius of the attocell R increases or the field of view Ψ_c decreases.

From a practical point of view, the above observation can be explained as follows. Recall that

$$\begin{aligned} F_{\cos(\psi)}(\cos(\Psi_c)) &= \Pr\left(\cos(\psi) \leq \cos(\Psi_c)\right) \\ &= \Pr\left(H \leq 0\right), \end{aligned} \tag{38}$$

which is literally the outage probability of the LiFi system, i.e., the probability that the UE is not connected to the AP even when it is inside the attocell. Obviously, for large values of R or small values of Ψ_c, the probability that the UE is

not connected to the AP increases. This is mainly due to the effects the random location of the user along with the random orientation of the UE and it explains the poor BER performance in this case.

The question that may come to mind here is how can one enhance the performance of the LiFi system under such a realistic environment? Recently, some practical solutions have been proposed in the literature to alleviate the effects of the random behaviour of LiFi channels. These solutions include the use of MIMO LiFi systems along with transceiver designs that have high spatial diversity gains such as the multi-directional receiver (MDR) [39], [40], the omni-directional transceiver [49] and the angular diversity transceiver [50]. Alternatively, we propose in the following subsection a new design of indoor LiFi cellular systems that can alleviate the effects of the random location of the user along with the random orientation of the UE.

C. Design Consideration of Indoor LiFi Cellular Systems

The concept of indoor cellular systems has been introduced in practical LiFi systems, where multiple LiFi APs coordinate together and serve multiple users within the resulting illuminated area [50]–[56]. Each LiFi AP creates an optical attocell and the respective illumination areas of the adjacent attocells overlap with each other. Consider the indoor LiFi cellular system shown in Fig. 10, which consists of five APs that correspond to small and adjacent attocells, where each has a radius R_c. The distance between the AP of the attocell in the middle (green attocell), which we refer to as the reference attocell, and the APs of the remaining adjacent attocells is D_c. Let us assume that a user is located within the reference attocell, where all five APs are cooperating and coordinating together to serve this user by transmitting the same signal. One way to reduce the outage probability of the user, i.e., the probability that it is not connected to at least one of the APs, is through a well designed attocells radius R_c and APs spacing D_c that guarantee a maximum target probability of error P_e^{th}, without any handover protocol between the different APs.

In this context, Fig. 11 presents the BER performance of a user that is located within the reference attocell, where the field of view of the UE is $\Psi_c = 60°$. Both stationary and mobile cases are considered and different values of R_c and D_c are evaluated. By comparing the results of this figure and those of Fig. 8, for the case when $R = 1$ m for example, we can see how the coexisting APs can significantly improve the BER performance of the system. In addition, we remark from Fig. 11 that the choice of (R_c, D_c) has also a big impact on the BER performance. For example, for the case of a stationary user, the best choice among the considered values is $(R_c, D_c) = (1\text{m}, 1.5\text{m})$, whereas for the case of a mobile user, the best choice is $(R_c, D_c) = (1\text{m}, 1\text{m})$. Overall, for a target probability of error $P_e^{\text{th}} = 3.8 \times 10^{-3}$, we conclude that the choice $(R_c, D_c) = (1\text{m}, 1\text{m})$ is the best choice that guarantees the target performance jointly for both stationary and mobile users. Obviously, the optimal (R_c, D_c) depends on the geometry of the attocells and the parameters of the UE as well, such as the height of the APs h_{a} and the height of the UE h_{u}. This problem will be investigated in future work.

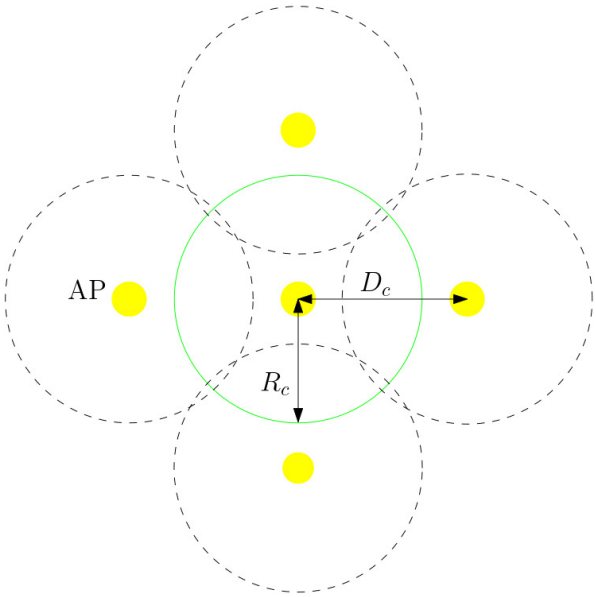

(a) Top view.

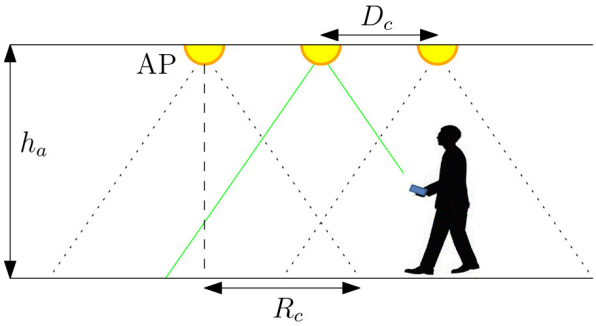

(b) Horizontal view.

Fig. 10. An indoor multi-cell LiFi system.

VI. Conclusions and Future Works

In this paper, novel, realistic, and measurement-based channel models for indoor LiFi systems have been proposed. The statistics of the LOS channel gain are derived for the case of stationary and mobile users, where the LiFi receiver is assumed to be randomly oriented. For stationary users, the MTL and the MB models were proposed, whereas for the case of mobile users, the SMTG and SMB models were proposed. The accuracy of each model was evaluated using the KSD. In addition, the effect of random orientation and spatial distribution of users on the error performance of users was investigated based on the derived models. Our results showed that the random behaviour and motion of users has strong effect on the LOS channel gain. Therefore, we proposed a novel design of indoor LiFi MIMO systems in order to guarantee the required reliability performance for reliable communication links.

The channel models proposed in this paper, albeit being fundamental and original, they serve as a starting point for developing realistic transmission techniques and transceiver designs tailored to real-world set-ups in an effort to bring the deployment of LiFi systems closer than ever. Thus, investigating optimal transceiver designs and cellular architectures based

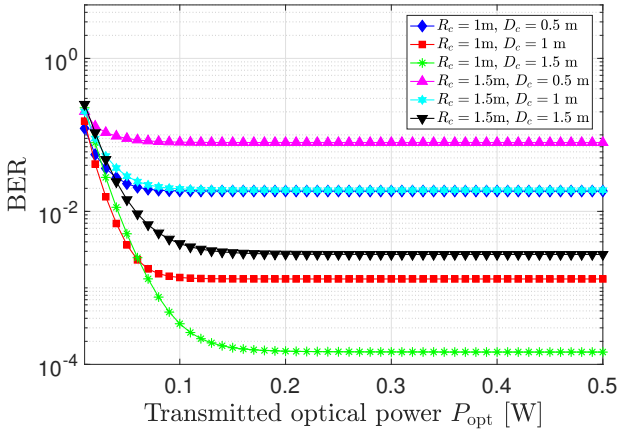

(a) Stationary user.

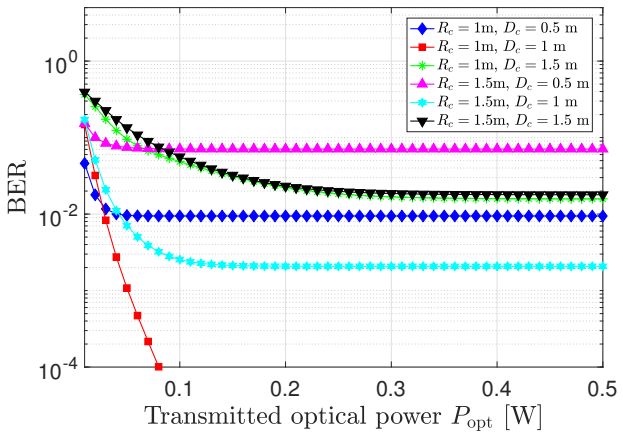

(b) Mobile user.

Fig. 11. BER performance of OOK modulation versus the transmitted optical power for stationary and mobile users when $\Psi_c = 60°$.

on the derived channel models that can meet the high demands of 5G and beyond in realistic communication environment can be considered as a future research direction. In addition, the derived channel models are intended for downlink communication in indoor LiFi environments. Therefore, deriving similar models for uplink transmission and for outdoor environments should also be considered in future work.

ACKNOWLEDGMENT

M. A. Arfaoui and C. Assi acknowledge the financial support from the Natural Sciences and Engineering Research Council of Canada (NSERC), Fonds Québécois de la Recherche sur la Nature et les Technologies (FQRNT) and from Concordia University. M. D. Soltani and M. Safari acknowledge financial support from the Engineering and Physical Sciences Research Council (EPSRC) under program grant EP/S016570/1 'Terabit Bidirectional Multi-User Optical Wireless System (TOWS) for 6G LiFi'. A. Ghrayeb is supported in part by Qatar National Research Fund under NPRP Grant NPRP8-052-2-029 and in part by FQRNT. H. Haas acknowledges the financial support from the Wolfson Foundation and Royal Society. He also gratefully acknowledges financial support by the Engineering and Physical Sciences Research Council (EPSRC).

APPENDIX A
PROOF OF THEOREM 1

At first, let us determine the range of the LOS channel gain H. Recall that H is expressed as

$$H = H_0 \frac{(h_a - h_u)^m \cos(\psi)}{l^{m+2}} \times \mathcal{U}_{[\cos(\Psi_c),0]}\left(\cos\left(\psi\right)\right), \quad (39)$$

where $\cos(\psi) = \frac{r\cos(\Omega-\alpha)\sin(\theta)+(h_a-h_u)\cos(\theta)}{l}$. Since $\Psi_c \in [0, \frac{\pi}{2}]$, we have $H \geq 0$ and the minimum value of H is equal to $h_{\min} = 0$. A set of values that can yield in $h_{\min} = 0$ is given as $l = l_{\min}$, $\Omega - \alpha = \pm k\frac{\pi}{2}$ s.t. $k = 1, 3$ and $\theta \geq \Psi_c$, which corresponds to the case where $\cos\left(\psi\right) \leq \cos\left(\Psi_c\right)$. On the other hand, the maximum value of H is equal to $h_{\max} = \frac{H_0}{(h_a-h_u)^2}$. A set of values that can yield in $h_{\max}$ is expressed as $l = h_a - h_u$, $\Omega - \alpha = \pm\frac{\pi}{2}$ s.t. $k = 1, 3$ and $\theta = 0$, which corresponds to the case where $\cos\left(\psi\right) = 0$.

The CDF of the LOS channel gain is expressed as shown in equation (40) on top of the next page, where $a^{'}(\theta) = \sin(\theta)$, $b^{'}(\theta) = (h_a - h_u)\cos(\theta)$ and the function I_H is expressed as

$$\begin{aligned} I_H\left(\theta, l\right) = & F_{\cos(\Omega-\alpha)}\left(\frac{l^{m+3}h - b(\theta)}{a(\theta)\sqrt{l^2-(h_a-h_u)^2}}\right) \\ & - F_{\cos(\Omega-\alpha)}\left(\frac{d\cos(\Psi_c) - b^{'}(\theta)}{a^{'}(\theta)\sqrt{l^2-(h_a-h_u)^2}}\right). \end{aligned} \quad (41)$$

Equality (40f) follows from the fact that the conditional probability under the integral in (40e) is not null if and only if $\frac{d\cos(\Psi_c)-b^{'}(\theta)}{a^{'}(\theta)\sqrt{l^2-(h_a-h_u)^2}} \leq \frac{l^{m+3}h-b(\theta)}{a(\theta)\sqrt{l^2-(h_a-h_u)^2}}$, i.e., $\left(\frac{H_0(h_a-h_u)^m\cos\Psi_c}{h}\right)^{\frac{1}{m+2}} \leq l$. Or, l is constrained within the range $[l_{\min}, l_{\max}]$. Therefore, the conditional probability in (40e) is not null if and only if $l \in [l^*_{\min}(h), l_{\max}]$, where $l^*_{\min}(h) = \max\left(l_0(h), l_{\min}\right)$ such that $l_0(h) = \left(\frac{H_0(h_a-h_u)^m\cos(\Psi_c)}{h}\right)^{\frac{1}{m+2}}$. Additionally, since l_0 should be always lower than $l_{\max}$, we conclude that the channel gain h under the integral in (40f) should satisfy $h^*_{\min} \leq h$, where $h^*_{\min} = \frac{H_0(h_a-h_u)^m\cos(\Psi_c)}{l^{m+2}_{\max}} \in [h_{\min}, h_{\max}]$. Furthermore, $F_{\cos(\psi)}(\cos(\Psi_c))$ in (40) is expressed as shown in (42) on top of next page. Based on this, the corresponding PDF of the LOS channel gain H is obtained by differentiating equality (40f) with respect to h. Using Leibniz integral rule for differentiation, the PDF of the LOS channel gain H is expressed as shown in (43) on top of next page. for $h \in [h^*_{\min}, h^*_{\max}]$, and 0 otherwise, such that $h^*_{\max} = h_{\max}\cos(\Psi_c) \in [h_{\min}, h_{\max}]$. This completes the proof.

APPENDIX B
PROOF OF THEOREM 2

Based on the results of Theorem 1, the PDF of the LOS channel gain H is given by

$$\begin{aligned} & f_H(h) \\ & = g_H(h)\mathcal{U}\left(h^*_{\min}, h_{\max}\right) + F_{\cos(\psi)}(\cos(\Psi_c))\delta(h) \\ & = \left(1 - F_{\cos(\psi)}(\cos(\Psi_c))\right) f_Z(h) + F_{\cos(\psi)}(\cos(\Psi_c))\delta(h), \end{aligned} \quad (44)$$

$$F_H(h) = \Pr\left(H \le h\right) \tag{40a}$$

$$= \Pr\left(\left(a(\theta)\frac{\sqrt{l^2-(h_a-h_u)^2}}{l^{m+3}}\cos(\Omega-\alpha) + \frac{b(\theta)}{l^{m+3}}\right) \times \mathbb{1}\left(\cos(\psi) > \cos(\Psi_c)\right) \le h\right) \tag{40b}$$

$$= \Pr\left(a(\theta)\frac{\sqrt{l^2-(h_a-h_u)^2}}{l^{m+3}}\cos(\Omega-\alpha) + \frac{b(\theta)}{l^{m+3}} \le h, 0 \le \psi \le \Psi_c\right) + \Pr\left(0 \le h, \Psi_c \le \psi\right) \tag{40c}$$

$$= \Pr\left(a(\theta)\frac{\sqrt{l^2-(h_a-h_u)^2}}{l^{m+3}}\cos(\Omega-\alpha) + \frac{b(\theta)}{l^{m+3}} \le h, \cos(\Psi_c) \le \cos(\psi)\right) + \Pr\left(0 \le h, \cos(\psi) \le \cos(\Psi_c)\right) \tag{40d}$$

$$= \int_{l_{\min}}^{l_{\max}}\int_0^{\frac{\pi}{2}} \Pr\left(\frac{d\cos(\Psi_c) - b^{'}(\theta)}{a^{'}(\theta)\sqrt{l^2-(h_a-h_u)^2}} \le \cos(\Omega-\alpha) \le \frac{l^{m+3}h - b}{a(\theta)\sqrt{l^2-(h_a-h_u)^2}}\middle|\theta, l\right) f_\theta(\theta) f_l(l)\mathrm{d}\theta\mathrm{d}l \tag{40e}$$

$$+ F_{\cos(\psi)}(\cos(\Psi_c))\mathcal{U}_{[0,\infty]}(h)$$

$$= \int_{l^*_{\min}(h)}^{l_{\max}}\int_0^{\frac{\pi}{2}} I_H\left(\theta, l\right) f_\theta(\theta) f_l(l)\mathrm{d}\theta\mathrm{d}l + F_{\cos(\psi)}(\cos(\Psi_c))\mathcal{U}_{[0,\infty]}(h), \tag{40f}$$

$$F_{\cos(\psi)}(\cos(\Psi_c)) = \Pr\left(\cos(\psi) \le \cos(\Psi_c)\right) \tag{42a}$$

$$= \int_{l_{\min}}^{l_{\max}}\int_0^{\frac{\pi}{2}} F_{\cos(\Omega-\alpha)}\left(\frac{d\cos(\Psi_c) - (h_a-h_u)\cos(\theta)}{\sin(\theta)\sqrt{l^2-(h_a-h_u)^2}}\right) f_\theta(\theta) f_l(l)\mathrm{d}\theta\mathrm{d}l. \tag{42b}$$

$$f_H(h) = \frac{\partial}{\partial h}\left[\Pr\left(H \le h\right)\right] \tag{43a}$$

$$= \int_{l^*_{\min}}^{l_{\max}}\int_0^{\frac{\pi}{2}} \frac{l^{m+3}}{a(\theta)\sqrt{l^2-(h_a-h_u)^2}} f_{\cos(\Omega-\alpha)}\left(\frac{l^{m+3}h - b(\theta)}{a(\theta)\sqrt{l^2-(h_a-h_u)^2}}\right) f_\theta(\theta) f_l(l)\mathrm{d}\theta\mathrm{d}l \tag{43b}$$

$$+ v(h)\int_0^{\frac{\pi}{2}} J_H\left(\theta, l\right) f_\theta(\theta)\mathrm{d}\theta + F_{\cos(\psi)}(\cos(\Psi_c))\delta(h),$$

---

where f_Z is a PDF, with support range $[h^*_{\min}, h_{\max}]$. The PDF f_Z is associated to the random variable Z that is expressed as $Z = XY$, where $X = \frac{c}{l^{m+2}}$ such that $c = H_0\left(h_{\rm a} - h_{\rm u}\right)^m$ and $Y = \cos\left(\psi\right)$ for $\psi \in [0, \Psi_c]$. Note that X and Y are two random variables that reflect the effects of the random spatial distribution of the user and the random orientation of the UE on the LOS channel gain, respectively. For the case of stationary users, and using the PDF transformation of random variables, the PDF of the random variable X is expressed as

$$\begin{aligned} f_X(x) &= \frac{c^{\frac{1}{m+2}}}{(m+2)}\left(\frac{1}{x}\right)^{\frac{m+3}{m+2}} f_d\left(\left(\frac{c}{x}\right)^{\frac{1}{m+2}}\right) \\ &= \frac{2c^{\frac{2}{m+2}}}{R^2(m+2)}\left(\frac{1}{x}\right)^{\frac{m+4}{m+2}} \mathcal{U}_{[c/l^{m+2}_{\max}, c/l^{m+2}_{\min}]}(x). \end{aligned} \tag{45}$$

Obviously, X and Y are correlated since they are a function of the distance l, which is also a random variable. However, such correlation can be weak in most of the cases. In fact, for high values of l, the effect of the random orientation on the LOS channel gain H is negligible compared to the one of the distance, whereas for the case of low values of l, the effect of the distance is negligible compared to the one of random orientation. Due to this, as an approximation, we assume that the random variables X and Y are uncorrelated. Based on this, using the theorem of the PDF of the product of random variables [57], the PDF of the random variable Z can be approximated as

$$\begin{aligned} f_Z(h) &\approx \int_{y_{\min}(h)}^{y_{\max}(h)} f_X\left(\frac{h}{y}\right) f_Y\left(y\right)\frac{\mathrm{d}y}{y} \\ &= \left(\frac{1}{h}\right)^{\frac{m+4}{m+2}} \int_{y_{\min}(h)}^{y_{\max}(h)} \frac{2c^{\frac{2}{m+2}}}{R^2(m+2)} y^{\frac{2}{m+2}} f_Y\left(y\right)\mathrm{d}y, \end{aligned} \tag{46}$$

where f_Y denotes the PDF of the random variable Y and it is given in (19) and (22) of [34]. Based on this, the PDF f_Z has the form $f_Z(h) \approx \frac{1}{h^\nu}\tilde{f}(h)$, where $\nu > 0$ and $\tilde{f}$ is a function with support range $[h^*_{\min}, h_{\max}]$ that is expressed as

$$\tilde{f}(h) = \int_{y_{\min}(h)}^{y_{\max}(h)} \frac{2c^{\frac{2}{m+2}}}{R^2(m+2)} y^{\frac{2}{m+2}} f_Y\left(y\right)\mathrm{d}y. \tag{47}$$

Consequently, by substituting $f_Z(h)$ in (47) by its expression and defining the function g, for $h \in [h^*_{\min}, h_{\max}]$, as $g(h) = \left(1 - F_{\cos(\psi)}(\cos(\Psi_c))\right)\tilde{f}(h)$, we obtain the result of Theorem 2, which completes the proof.

APPENDIX C
PROOF OF THEOREM 3

Using the same notation adopted in Appendix B, the PDF of the random variable X for the case of mobile users is

expressed as

$$f_X(x) = \frac{c^{\frac{1}{m+2}}}{(m+2)} \left(\frac{1}{x}\right)^{\frac{m+3}{m+2}} f_d\left(\left(\frac{c}{x}\right)^{\frac{1}{m+2}}\right) = \sum_{i=1}^{3} \frac{a_i c^{b_i+\frac{2}{m+2}}}{(m+2)R^{b_i+1}} \left(\frac{1}{x}\right)^{b_i+\frac{m+4}{m+2}} \mathcal{U}_{\left[c/l_{\max}^{m+2}, c/l_{\min}^{m+2}\right]}(x). \tag{48}$$

Therefore, the PDF of the random variable Z can be approximated by

$$f_Z(h) \approx \int_{y_{\min}(h)}^{y_{\max}(h)} f_X\left(\frac{h}{y}\right) f_Y(y) \frac{\mathrm{d}y}{y} = \sum_{i=1}^{3} \left(\frac{1}{h}\right)^{b_i+\frac{m+4}{m+2}} \int_{y_{\min}(h)}^{y_{\max}(h)} \left[\frac{a_i c^{b_i+\frac{2}{m+2}}}{(m+2)R^{b_i+1}} \times y^{b_i+\frac{m+4}{m+2}} f_Y(y)\right] \mathrm{d}y, \tag{49}$$

which has the form $f_Z(h) \approx \sum_{j=1}^{3} \frac{1}{z^{\nu_i}} \tilde{f}_j(h)$, where, for $j = 1, 2, 3$, $\nu_j > 0$ and $\tilde{f}_j$ is a function with support range $[h_{\min}^*, h_{\max}]$ that is expressed as

$$\tilde{f}_j(h) = \int_{y_{\min}(h)}^{y_{\max}(h)} \left[\frac{a_i c^{b_i+\frac{2}{m+2}}}{(m+2)R^{b_i+1}} y^{b_i+\frac{m+4}{m+2}} f_Y(y)\right] \mathrm{d}y. \tag{50}$$

Consequently, by substituting $f_Z(h)$ in (47) by its expression and defining $g_j(h)$, for $j = 1, 2, 3$ and for $h \in [h_{\min}^*, h_{\max}]$, as $g_j(h) = \left(1 - F_{\cos(\psi)}(\cos(\Psi_c))\right) \tilde{f}_j(h)$, we obtain the result of Theorem 3, which completes the proof.

Appendix D
Proof of Corollary 1

Based on the PDF of the LOS channel gain H provided in Theorem 1 and the expression of the probability of error of M-pulse amplitude modulation [58], [59], the average probability of error of the considered LiFi system is expressed as

$$P_e = \int_{h_{\min}}^{h_{\max}} f_H(h) P_{e,h}(P_{\text{opt}}, h) \mathrm{d}h \tag{51a}$$

$$= \int_{h_{\min}^*}^{h_{\max}} g_H(h) \frac{2(M-1)}{M} \mathcal{Q}\left(\frac{hP_{\text{opt}}}{\sigma(M-1)}\right) \mathrm{d}h + F_{\cos(\psi)}(\cos(\Psi_c)) \int_{h_{\min}}^{h_{\max}} \delta(h) \mathcal{Q}\left(\frac{hP_{\text{opt}}}{\sigma(M-1)}\right) \mathrm{d}h, \tag{51b}$$

where $P_{e,h}(P_{\text{opt}}, h)$ is the instantaneous probability of error for a given channel gain h and $\gamma_{\text{TX}} = \frac{P_{\text{elec}}}{\sigma^2} = \frac{P_{\text{opt}}^2}{\sigma^2}$ is the transmitted SNR, such that P_{elec} is the transmitted electrical signal and σ^2 is the average noise power at the receiver. Now, since the function $h \mapsto g_H(h) \frac{2(M-1)}{M} \mathcal{Q}\left(\frac{hP_{\text{opt}}}{\sigma(M-1)}\right)$ is a smooth function within $[h_{\min}^*, h_{\max}]$, and using the Lebesgue's dominated convergence theorem, we get

$$\lim_{P_{\text{opt}} \to \infty} \int_{h_{\min}}^{h_{\max}} g_H(h) \frac{2(M-1)}{M} \mathcal{Q}\left(\frac{hP_{\text{opt}}}{\sigma(M-1)}\right) \mathrm{d}h = \int_{h_{\min}}^{h_{\max}} \lim_{P_{\text{opt}} \to \infty} g_H(h) \frac{2(M-1)}{M} \mathcal{Q}\left(\frac{hP_{\text{opt}}}{\sigma(M-1)}\right) \mathrm{d}h = 0. \tag{52}$$

Furthermore, since $h_{\min} = 0$, we have $\int_{h_{\min}}^{h_{\max}} \delta(h) \mathcal{Q}\left(\frac{hP_{\text{opt}}}{\sigma(M-1)}\right) \mathrm{d}h = \mathcal{Q}(0) = \frac{1}{2}$, which implies that $\lim_{P_{\text{opt}} \to \infty} \int_{h_{\min}}^{h_{\max}} \delta(h) \mathcal{Q}\left(\frac{hP_{\text{opt}}}{\sigma(M-1)}\right) \mathrm{d}h = \frac{1}{2}$. Therefore, we conclude that $\lim_{P_{\text{opt}} \to \infty} P_e(P_{\text{opt}}) = \frac{F_{\cos(\psi)}(\cos(\Psi_c))}{2}$, which completes the proof.

References

[1] C. V. Networking, "Cisco global cloud index: Forecast and methodology, 2016–2021," White Paper, Cisco, San Jose, CA, USA Nov. 2019.

[2] J. G. Andrews, S. Buzzi, W. Choi, S. V. Hanly, A. Lozano, A. C. Soong, and J. C. Zhang, "What will 5G be?" *IEEE J. on selected areas in commun.*, vol. 32, no. 6, pp. 1065–1082, Jun. 2014.

[3] M. Shafi, A. F. Molisch, P. J. Smith, T. Haustein, P. Zhu, P. Silva, F. Tufvesson, A. Benjebbour, and G. Wunder, "5G: A tutorial overview of standards, trials, challenges, deployment, and practice," *IEEE J. on selected areas in commun.*, vol. 35, no. 6, pp. 1201–1221, Apr. 2017.

[4] P. Pirinen, "A brief overview of 5G research activities," in *Proc. IEEE 5GU*, Akaslompolo, Finland, Nov. 2014.

[5] A. Al-Fuqaha, M. Guizani, M. Mohammadi, M. Aledhari, and M. Ayyash, "Internet of things: A survey on enabling technologies, protocols, and applications," *IEEE Commun. Surveys & Tutorials*, vol. 17, no. 4, pp. 2347–2376, Jun. 2015.

[6] M. R. Palattella, M. Dohler, A. Grieco, G. Rizzo, J. Torsner, T. Engel, and L. Ladid, "Internet of things in the 5G era: Enablers, architecture, and business models," *IEEE JSAC*, vol. 34, no. 3, pp. 510–527, Feb. 2016.

[7] D. Tsonev, S. Videv, and H. Haas, "Towards a 100 Gb/s visible light wireless access network," *Optics express*, vol. 23, no. 2, pp. 1627–1637, Jan. 2015.

[8] N. Bhushan, J. Li, D. Malladi, R. Gilmore, D. Brenner, A. Damnjanovic, R. Sukhavasi, C. Patel, and S. Geirhofer, "Network densification: the dominant theme for wireless evolution into 5G," *IEEE Commun. Magazine*, vol. 52, no. 2, pp. 82–89, Feb. 2014.

[9] X. Ge, S. Tu, G. Mao, C.-X. Wang, and T. Han, "5G ultra-dense cellular networks," *IEEE Wireless Commun.*, vol. 23, no. 1, pp. 72–79, Mar. 2016.

[10] H. Haas, L. Yin, Y. Wang, and C. Chen, "What is LiFi?" *Journal of lightwave technology*, vol. 34, no. 6, pp. 1533–1544, 2015.

[11] I. Tavakkolnia, C. Chen, R. Bian, and H. Haas, "Energy-efficient adaptive MIMO-VLC technique for indoor LiFi applications," in *Proc. IEEE ICT*, St. Malo, France, Hun. 2018.

[12] S. Wu, H. Wang, and C.-H. Youn, "Visible light communications for 5G wireless networking systems: from fixed to mobile communications," *IEEE Network*, vol. 28, no. 6, pp. 41–45, Nov. 2014.

[13] D. Karunatilaka, F. Zafar, V. Kalavally, and R. Parthiban, "LED based indoor visible light communications: State of the art," *IEEE Commun. Surveys & Tutorials*, vol. 17, no. 3, pp. 1649–1678, Mar. 2015.

[14] P. H. Pathak, X. Feng, P. Hu, and P. Mohapatra, "Visible light communication, networking, and sensing: A survey, potential and challenges," *IEEE Commun. Surveys & tutorials*, vol. 17, no. 4, pp. 2047–2077, Sep. 2015.

[15] M. Obeed, A. M. Salhab, M.-S. Alouini, and S. A. Zummo, "On optimizing VLC networks for downlink multi-user transmission: A survey," *IEEE Communications Surveys & Tutorials*, vol. 21, no. 3, pp. 2947 – 2976, Mar. 2019.

[16] G. Pan, J. Ye, and Z. Ding, "On secure VLC systems with spatially random terminals," *IEEE Communications Letters*, vol. 21, no. 3, pp. 492–495, 2016.

[17] J.-Y. Wang, C. Liu, J.-B. Wang, Y. Wu, M. Lin, and J. Cheng, "Physical-layer security for indoor visible light communications: Secrecy capacity analysis," *IEEE Trans. on Commun.*, vol. 66, no. 12, pp. 6423–6436, Dec. 2018.

[18] L. Yin, W. O. Popoola, X. Wu, and H. Haas, "Performance evaluation of non-orthogonal multiple access in visible light communication," *IEEE Trans. on Commun.*, vol. 64, no. 12, pp. 5162–5175, Sep. 2016.

[19] A. Gupta, N. Sharma, P. Garg, and M.-S. Alouini, "Cascaded FSO-VLC communication system," *IEEE Wireless Commun. Letters*, vol. 6, no. 6, pp. 810–813, Aug. 2017.

[20] S. Cho, G. Chen, and J. P. Coon, "Physical layer security in visible light communication systems with randomly located colluding eavesdroppers," *IEEE Wireless Commun. Letters*, vol. 7, no. 5, pp. 768 – 771, Oct. 2018.

[21] Y. Yapici and I. Guvenc, "Non-orthogonal multiple access for mobile vlc networks with random receiver orientation," in *Proc. IEEE Globecom*, Waikoloa, HI, USA, USA, Dec. 2019.

[22] K. Govindan, K. Zeng, and P. Mohapatra, "Probability density of the received power in mobile networks," *IEEE Trans. Wireless Commun.*, vol. 10, no. 11, pp. 3613–3619, Dec. 2011.

[23] V. A. Aalo, C. Mukasa, and G. P. Efthymoglou, "Effect of mobility on the outage and BER performances of digital transmissions over Nakagami-m fading channels," *IEEE Trans. Vehicular Tech.*, vol. 65, no. 4, pp. 2715–2721, Apr. 2016.

[24] A. Gupta and P. Garg, "Statistics of SNR for an Indoor VLC System and its Applications in System Performance," *IEEE Commun. Letters*, vol. 22, no. 9, pp. 1898 – 1901, Jul. 2018.

[25] M. A. Arfaoui, M. D. Soltani, I. Tavakkolnia, A. Ghrayeb, C. Assi, H. Haas, and M. Safari, "SNR Statistics for Indoor VLC Mobile Users with Random Orientation," in *Proc. IEEE ICC*, Shanghai, China, May. 2019.

[26] M. D. Soltani, X. Wu, M. Safari, and H. Haas, "Access point selection in li-fi cellular networks with arbitrary receiver orientation," in *Proc. IEEE ICC*, Valencia, Spain, 2016.

[27] M. D. Soltani, H. Kazemi, M. Safari, and H. Haas, "Handover Modeling for Indoor Li-Fi Cellular Networks: The Effects of Receiver Mobility and Rotation," in *Proc. IEEE WCNC*, San Fransisco, USA, Mar. 2017.

[28] A. A. Purwita, M. D. Soltani, M. Safari, and H. Haas, "Handover Probability of Hybrid LiFi/RF-Based Networks with Randomly-Oriented Devices," in *Proc. IEEE VTC*, Porto, Portugal, Jun Jun. 2018.

[29] J.-Y. Wang, Q.-L. Li, J.-X. Zhu, and Y. Wang, "Impact of receiver's tilted angle on channel capacity in VLCs," *Electronics Letters*, vol. 53, no. 6, pp. 421–423, Mar. 2017.

[30] J.-Y. Wang, J.-B. Wang, B. Zhu, M. Lin, Y. Wu, Y. Wang, and M. Chen, "Improvement of BER performance by tilting receiver plane for indoor visible light communications with input-dependent noise," in *Proc. IEEE ICC*, Paris, France, May 2017.

[31] Z. Wang, C. Yu, W.-D. Zhong, and J. Chen, "Performance improvement by tilting receiver plane in M-QAM OFDM visible light communications," *Optics express*, vol. 19, no. 14, pp. 13 418–13 427, Jun. 2011.

[32] A. A. Matrawy, M. A. El-Shimy, M. R. Rizk, and Z. A. El-Sahn, "Optimum angle diversity receivers for indoor single user MIMO visible light communication systems," in *Proc. Asia Communications and Photonics Conference*. Wuhan, China: Optical Society of America, 2016.

[33] Y. S. Eroğlu, Y. Yapıcı, and I. Güvenç, "Impact of random receiver orientation on visible light communications channel," *IEEE Transactions on Commun.*, vol. 67, no. 2, pp. 1313–1325, Nov. 2018.

[34] M. D. Soltani, A. A. Purwita, Z. Zeng, H. Haas, and M. Safari, "Modeling the Random Orientation of Mobile Devices: Measurement, Analysis and LiFi Use Case," *IEEE Trans. Commun.*, vol. 67, no. 3, pp. 2157–2172, 2019.

[35] A. A. Purwita, M. D. Soltani, M. Safari, and H. Haas, "Impact of terminal orientation on performance in LiFi systems," in *Proc. IEEE WCNC*, Barcelona, Spain, Apr. 2018.

[36] Z. Zeng, M. D. Soltani, H. Haas, and M. Safari, "Orientation Model of Mobile Device for Indoor VLC and Millimetre Wave Systems," in *Proc. IEEE VTC*, Chicago, USA, Aug. 2018.

[37] M. D. Soltani, "Analysis of Random Orientation and User Mobility in LiFi Networks," *The University of Edinburgh*, 2019.

[38] M. D. Soltani, A. A. Purwita, I. Tavakkolnia, H. Haas, and M. Safari, "Impact of device orientation on error performance of LiFi systems," *IEEE Access*, vol. 7, pp. 41 690–41 701, Mar. 2019.

[39] M. D. Soltani, M. A. Arfaoui, I. Tavakkolnia, A. Ghrayeb, C. Assi, H. Haas, M. Hasna, and M. Safari, "Bidirectional optical spatial modulation for mobile users: Towards a practical design for lifi systems," *IEEE JSAC SI Spatial Modulation in Emerging Wireless Systems*, vol. 37, no. 9, pp. 2069 – 2086, Aug. 2019.

[40] I. Tavakkolnia, M. D. Soltani, M. A. Arfaoui, , A. Ghrayeb, C. Assi, M. Safari, and H. Haas, "MIMO System with Multi-directional Receiver in Optical Wireless Communications," in *Proc. IEEE ICC*, Shanghai, China, May. 2019.

[41] C. Chen, M. D. Soltani, M. Safari, A. A. Purwita, X. Wu, and H. Haas, "An Omnidirectional User Equipment Configuration to Support Mobility in LiFi Networks," in *Proc. IEEE ICC*, Shanghai, China, May. 2019.

[42] M.-A. Arfaoui, Z. Rezki, A. Ghrayeb, and M. S. Alouini, "On the secrecy capacity of MISO visible light communication channels," in *Proc. IEEE Globecom*, Washington DC, USA, Dec. 2016.

[43] L. Zeng, D. O'Brien, H. Le-Minh, K. Lee, D. Jung, and Y. Oh, "Improvement of data rate by using equalization in an indoor visible light communication system," in *Proc. IEEE ICCSC*, Shanghai, China, Jun. 2008.

[44] L. Zeng, D. C. O'Brien, H. Le Minh, G. E. Faulkner, K. Lee, D. Jung, Y. Oh, and E. T. Won, "High data rate multiple input multiple output (MIMO) optical wireless communications using white LED lighting," *IEEE J. Select. Areas in Commun.*, vol. 27, no. 9, pp. 1654 – 1662, Dec. 2009.

[45] M. A. Arfaoui, A. Ghrayeb, and C. Assi, "Secrecy rate closed-form expressions for the SISO VLC wiretap channel with discrete input signaling," *IEEE Commun. Letters*, vol. 22, no. 7, pp. 1382 – 1385, Apr. 2018.

[46] S. Tao, H. Yu, Q. Li, and Y. Tang, "Derivation and analysis of probability distribution of visible-light channel gain difference based on Lambertian radiation," *IEEE Commun. Letters*, vol. 24, no. 2, pp. 371 – 375, Feb. 2020.

[47] Y. Yapıcı and I. Güvenç, "NOMA for VLC downlink transmission with random receiver orientation," *IEEE Trans. Communications*, vol. 67, no. 8, pp. 5558–5573, Apr. 2019.

[48] F. J. Massey Jr, "The kolmogorov-smirnov test for goodness of fit," *Journal of the American statistical Association*, vol. 46, no. 253, pp. 68–78, 1951.

[49] C. Chen, R. Bian, and H. Haas, "Omnidirectional transmitter and receiver design for wireless infrared uplink transmission in LiFi," in *Proc. IEEE ICC*, Kansas City, Missouri, USA, May 2018.

[50] C. Chen, W.-D. Zhong, H. Yang, S. Zhang, and P. Du, "Reduction of SINR fluctuation in indoor multi-cell VLC systems using optimized angle diversity receiver," *Journal of Lightwave Technology*, vol. 36, no. 17, pp. 3603–3610, May 2018.

[51] C. Chen, D. Tsonev, and H. Haas, "Joint transmission in indoor visible light communication downlink cellular networks," in *Proc. IEEE Globecom*, Atlanta, GA, USA, Dec. 2013.

[52] H. Ma, L. Lampe, and S. Hranilovic, "Coordinated broadcasting for multiuser indoor visible light communication systems," *IEEE Trans. Communications*, vol. 63, no. 9, pp. 3313–3324, Jul. 2015.

[53] T. V. Pham, H. Le Minh, and A. T. Pham, "Multi-cell VLC: Multi-user downlink capacity with coordinated precoding," in *IEEE ICC*, Paris, France, May 2017.

[54] H. Yang, C. Chen, W.-D. Zhong, and A. Alphones, "Joint precoder and equalizer design for multi-user multi-cell MIMO VLC systems," *IEEE Transactions on Vehicular Tech.*, vol. 67, no. 12, pp. 11 354–11 364, Oct. 2018.

[55] S. Tao, H. Yu, Q. Li, and Y. Tang, "Performance analysis of user association strategy based on power-domain non-orthogonal multiple access in visible light communication multi-cell networks," *EURASIP Journal on Wireless Communications and Networking*, vol. 2020, no. 1, pp. 1–13, Apr. 2020.

[56] M. W. Eltokhey, M. A. Khalighi, A. S. Ghazy, and S. Hranilovic, "Hybrid NOMA and ZF Pre-coding Transmission for Multi-Cell VLC Networks," *IEEE Open Journal of the Communications Society*, Apr. 2020.

[57] A. G. Glen, L. M. Leemis, and J. H. Drew, "Computing the distribution of the product of two continuous random variables," *J. of Computational statistics & data analysis*, vol. 44, no. 3, pp. 451–464, Jan. 2004.

[58] J. M. Kahn and J. R. Barry, "Wireless infrared communications," *Proc. of the IEEE*, vol. 85, no. 2, pp. 265–298, Feb. 1997.

[59] C.-C. Yeh and J. R. Barry, "Approximate minimum bit-error rate equalization for pulse-amplitude and quadrature-amplitude modulation," in *Proc. IEEE ICC*, Atlanta, GA, USA, Jun. 1998.

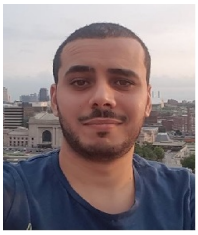

Mohamed Amine Arfaoui (S'16) received the B.E. degree in electrical and computer engineering from the École Polytechnique de Tunisie, Tunisia, in 2015, and the M.Sc. degree in information systems engineering from Concordia University, Montreal, QC, Canada, in 2017. He is currently pursuing the Ph.D. degree in information systems engineering with Concordia University, Montreal. His research interests include communication theory, optical communications and physical layer security.

Mohammad Dehghani Soltani (S'15) received the M.Sc. degree from the Department of electrical engineering, Amirkabir University of Technology, Tehran, Iran, in 2012 and the Ph.D degree in electrical engineering from the University of Edinburgh, Edinburgh, UK, in 2019. During his MSc, he was studying wireless communications, MIMO coding and low complexity design of MIMO-OFDM systems. He worked for two years in the telecommunication industry in Iran. His PhD was funded by the British Engineering and Physical Sciences Research Council (EPSRC) Project TOUCAN. During his PhD, he was studying visible light communication, mobility and handover management in wireless cellular networks, resource allocation and user behavior modeling. He is currently a Research Associate with the LiFi Research and Development Centre at the University of Edinburgh, funded by EPSRC 'Terabit Bidirectional Multi-User Optical Wireless System (TOWS) for 6G LiFi'.

Iman Tavakkolnia (S'15, M'19) received the B.Sc. degree in telecommunication engineering from the University of Tehran, Tehran, Iran, in 2006, the M.Sc. degree in communication systems from the Sharif University of Technology, Tehran, in 2011, and the Ph.D. degree in electrical engineering from The University of Edinburgh, Edinburgh, U.K., in 2018,where he is currently a Research Associate with the LiFi Research and Development Centre. His research interests include communication theory, optical fiber communication, and visible light communication.

Ali Ghrayeb received the Ph.D. degree in electrical engineering from The University of Arizona, Tucson, AZ, USA, in 2000. He is currently a Professor with the Department of Electrical and Computer Engineering, Texas A&M University at Qatar. Prior to his current position, he was a professor with the Department of Electrical and Computer Engineering, Concordia University, Montreal, Canada. He has coauthored two books and published over 200 journal and conference papers. His research interests include wireless and mobile communications, physical layer security, massive MIMO, and visible light communications. He served as an instructor or co-instructor in technical tutorials at several major IEEE conferences. He served as the Executive Chair for the 2016 IEEE WCNC conference. He has served on the editorial board of several IEEE and non-IEEE journals. He is a Fellow of the IEEE.

Chadi M. Assi received the Ph.D. degree from the City University of New York (CUNY) in 2003. He is currently a Full Professor at Concordia University. He was a recipient of the Prestigious Mina Rees Dissertation Award from CUNY in 2002 for his research on wavelength-division multiplexing optical networks. He is on the Editorial Board of IEEE Communications Surveys and Tutorials, the IEEE Transactions on Communications, and the IEEE Transactions on Vehicular Technologies. His current research interests are in the areas of network design and optimization, network modelling, and network reliability.

Majid Safari (S'08- M'11) received his Ph.D. degree in Electrical and Computer Engineering from the University of Waterloo, Canada in 2011. He also received his B.Sc. degree in Electrical and Computer Engineering from the University of Tehran, Iran, in 2003, M.Sc. degree in Electrical Engineering from Sharif University of Technology, Iran, in 2005. He is currently a Reader in the Institute for Digital Communications at the University of Edinburgh. Before joining Edinburgh in 2013, He held postdoctoral fellowship at Mc-Master University, Canada. Dr. Safari is currently an associate editor of IEEE Transactions on Communications and was the TPC co-chair of the 4th International Workshop on Optical Wireless Communication in 2015. His main research interest is the application of information theory and signal processing in optical communications including fiber-optic communication, free-space optical communication, visible light communication, and quantum communication.

Harald Haas (S'98-A'00-M'03-SM'16-F'17) received the Ph.D. degree from The University of Edinburgh in 2001. He is currently the Chair of Mobile Communications at The University of Edinburgh, and he is the Initiator, Co-Founder, and Chief Scientific Officer of pureLiFi Ltd., and the Director of the LiFi Research and Development Centre, The University of Edinburgh. He has authored 500 conference and journal papers. His main research interests are in optical wireless communications, hybrid optical wireless and RF communications, spatial modulation, and interference coordination in wireless networks. He is an Associate Editor of the IEEE Journal of Lightwave Technologies. He gave two TED Global talks "Wireless Data From Every light Bulb" and "Forget Wi-Fi: Meet the New Li-Fi Internet" which together have been downloaded more than 5.5 million times. In 2012 and 2017, he was a recipient of the prestigious Established Career Fellowship from the Engineering and Physical Sciences Research Council (EPSRC) in the U.K. In 2014, he was selected by EPSRC as one of ten Recognizing Inspirational Scientists and Engineers Leaders in the U.K. He was a co-recipient of the EURASIP Best Paper Award for the Journal on Wireless Communications and Networking in 2015 and the Jack Neubauer Memorial Award of the IEEE Vehicular Technology Society. In 2016, he received the Outstanding Achievement Award from the International Solid State Lighting Alliance. He was a co-recipient of recent best paper awards at VTC-Fall, 2013, VTC-Spring 2015, ICC 2016, ICC 2017 and ICC 2018. In 2019 he received the James Evans Avant Garde Award of the IEEE Vehicular Technology Society. Haas is a Fellow of the Royal Academy of Engineering.